POLITECNICO DI MILANO

SCUOLA INTERPOLITECNICA DI DOTTORATO

Doctoral Program in Bioengineering

Final Dissertation

Force sensing and display in robotic driven needles for minimally invasive surgery

Danilo De Lorenzo
738498

Tutor
Prof. Giancarlo Ferrigno

Supervisor
Elena De Momi, PhD

Co-ordinator of the Research Doctorate Course
Prof. Maria Gabriella Signorini

1st March 2012 - XXIV cycle

Abstract

MINIMALLY invasive surgical procedures, such as laparoscopy, have been facilitated by tele-operated robotic systems, which provide augmented dexterity in narrow spaces. However, the physical separation between the operating surgeon and the patient body does not provide the surgeon with direct force and tactile feedback. Together with costs and safety issues, one of the reasons that has prevented the proliferation of robotic devices inside the operating room is the need of changing the standard workflow of the surgical procedures and the standard instruments, together with the need of surgeon training. Needle insertion is a minimally invasive procedure, involving several applications such as blood sampling, anaesthesia, biopsy, brachytherapy, and placement of electrodes. Force feedback for needle insertion tasks has been widely investigated to build surgical simulators, but has not been translated into the real surgical scenario.

In this thesis, we studied and developed new methods for integrating force sensing with robotic devices, for needle insertion procedures, without requiring any changes in the standard surgical needle and in surgical workflow modality, thus increasing the intervention outcome, safety and performances with relative low costs. In particular, we developed sensors and sensing modalities integrated in the robotic devices, force control algorithms for force feedback enhancement and needle insertion task improvement and design of experimental protocol for testing and validation. Teleoperation and comanipulation control schemes were tested in custom made mock surgical environments, considering neurosurgical requirements as the envis-

aged clinical application. Both the operation schemes allowed to accurately identify small force differences when the needle is inserted into soft tissues. In the teleoperation scenario new force sensing modalities were integrated in a small linear piezo-driver with high positioning accuracy and proved to be suitable for the neurosurgical applications. In the comanipulation approach force feedback scaling and enhanced needle tip force perception were validated with human subject experiments and proved to be suitable for detecting small tissue property changes, thus increasing procedure accuracy and safety.

Attention was carefully paid to test the systems with mimicking soft tissue materials, whose mechanical characteristics are close to reality. The developed systems should be carefully tested in preclinical conditions, such as ex vivo biological tissues, to better evaluate clinical relevance, however we showed that enhanced force feedback can help the surgeon in a variety of different experimental conditions using different control modalities and force sensing principles.

Acknowledgements

When I started writing my thesis I was not sure when I was going to finish, but I was sure that I would have noticed it as soon as I would have started writing the first word of the most widely read section. And now, here we are.

First of all thanks to my family. Grazie a Giovanna e Pancrazio, Maria, Gianluca e nonna Concetta. Thanks for having grown in me the curiosity in the World and for not having stopped my continuous asking Why? when I was a child.

Thanks to my "academic family", the NearLab group, past and present members. Thanks to Giancarlo and Elena not only for being my supervisors, but for what you taught me in these years, for having showed me the sweet and the bitter of our work, but also for Elena's enthusiasm and for the Giancarlo's funny competitive nature even in drinking or playing games (or contemporary both of them). Thanks to NearLab mates for the pleasure of alternating scientific discussion with funny and stupid discussions, for the lunches in our small "Cucina", for coffee-breaks, hard sport matches, beautiful travels, procrastinations... Thanks to the rearguard Alberto, Emiliano, Claudia, Emilia A and Emilia B, Simona, Marta and to the new entries Mirko, Chiara and Elisa.

Thanks to prof. Moshe Shoham for hosting me in his Lab and thanks to Ilya and the guys of the Medical Robotics Lab for the nice Summer spent together.

I am grateful to Allison, for inviting me to the Haptics Lab and for mentoring me during the beautiful and mind-opening period in the States. Thanks to the Haptics lab mates and to Yoshi for the beautiful time spent together.

Thanks to Dana and Matteo for our scientific and philosophic discussions, for the lunch and the dinners laughing together, and mostly for ours dreaming coffee breaks.

Thanks to Francesca, my love. Thanks for your patience in carrying mine "it's a period" even if it's three years that "it's a period...". Thanks for having shared the USA experience with me (we will never forget it) and for sharing with me your life and our happiness. Thanks to Tiziana and Zia Piera for having "adopted" me. Thanks to my friends, for being that.

To my family

Contents

Contents

Acronyms

BC Back Clamp

FC Forward Clamp

FS Force Sensor

LA Linear Actuator

MIS Minimally Invasive Surgery

P Pushing element

PC Proportional Controller

PE Pushing element

RMIS Robotic Minimally Invasive Surgery

RMSE Root Mean Square Error

ROBOCAST ROBOt and sensors integration for Computer Assisted Surgery and Therapy

SG Strain Gauge

DOF Degree Of Freedom

JND Just Noticeable Difference

GP Gross Positioner

FP Fine Positioner

CHAPTER 1

Introduction

Over the last century, new technologies have drastically changed how the surgical procedures are performed (Figure 1.1). In the past, the surgeon could only open the body in order to look inside and reach the target of the intervention. Starting from the '80s, Minimally Invasive Surgery (MIS) allowed the surgery to be performed, through small incision (0.5-1.5cm). The surgeon can now see the target of the intervention using a small camera at the tip of the endoscope and look the real-time images on a monitor.

In the '90s, with the advent of the da Vinci® robot (Figure 1.1, on the right) research on Robotic Minimally Invasive Surgery (RMIS) allowed the surgeon to operate remotely, without having his/her hands close to the patient body and by means of an immersive 3D vision experience. If endoscopy revolutionized surgery decreasing the trauma to the patient, today RMIS adds the possibility to enhance surgeon's abilities in gestures execution (by tremor reduction, motion scaling...).

However, both for the MIS and for RMIS, surgeons lose their sense of touch, since their hands are no more directly in touch with the patient body. In robotics, the sense of touch is called

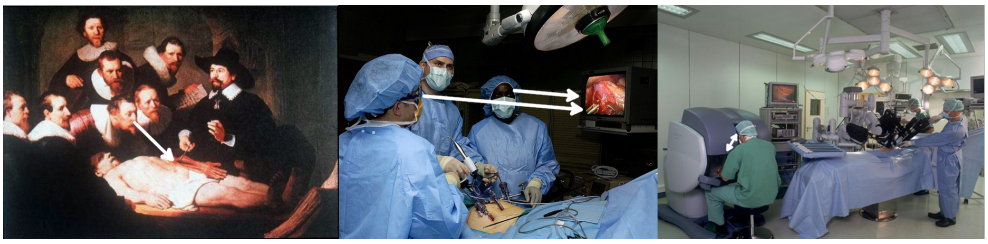

Figure 1.1: *History of Surgery towards mimimally invasive interventions. On the left, the "Anatomy Lesson of Dr. Tulp" by Rembrandt, in the center, an example of modern laparoscopic surgery, on the right, a modern robotic operating room equipped with the da Vinci® surgical platform. Technology introduced the possibility to perform surgery through small access to the body, but at the expenses of loosing tactile information and reducing operating field of view. From left to right, the picture shows also how the visual inspection and the effort in hand-eye coordination is changed*

haptics and refers to the force perceived by the surgeon hand due to the interactions between the robotic instruments and the soft tissue. Without haptic information in RMIS, the surgeon relies solely on visual feedback and the sense of touch is just represented by the mechanical interface (handles, mechanical inertia, friction) between the hands and the tissue. Haptics is broadly defined as real and simulated touch interactions between robots, humans, and real, remote, or simulated environments, in various combinations [70]. The goal of haptic in RMIS is to provide "transparency", in which the surgeon does not feel as if he is operating a remote device, but rather that his own hands are directly in contact with the patient. This requires sensors to acquire force and touch information, and haptic devices to display the information to the surgeon. Haptics includes information on force, temperature, pressure, vibrations, and texture, which can be difficult to acquire and display with high fidelity. In the 1990s, haptics research expanded significantly thanks to commercially available force feedback systems from companies such as SensAble Technologies, Inc. (Woburn, MA, USA), Immersion, Inc. (San Jose, CA, USA) and, more recently, Force Dimension (Nyon, Switzerland). Recent reviews of haptics in surgery are [75] [24].

In surgical tasks where fine manipulation of delicate tissues is required, the lack of tactile and force information increases the number of surgical errors and tissue damage to the patient. Giving to the surgeon the possibility to remotely feel the amount of force that he/she is applying on the tissue during the intervention is a challenging task because of the cost of adding force sensors to disposable and/or sterilizable instruments, the cost and the technical difficulties in

sensors miniaturization and the complexity of the control algorithms.

The goal of this thesis was to investigate new methodologies for the implementation of force sensing and force feedback in robotic driven needle insertion for RMIS. Furthermore, the benefit of the robotic systems not only in replicating the force perception but even in the enhancement of differential force perception was examined.

CHAPTER 2

Force sensing and display in Robotic Minimally Invasive Surgery (RMIS)

2.1 Force feedback and task performances in RMIS

Force feedback in RMIS allows the human operator to manipulate tissues as if his/her hands were in contact with the patient organs. For some applications, visual and auditory cues may be sufficient as tactile substitution, but for some others there are limitations such as worsening of performance in navigation [6], manipulation [77], and sense of presence [57]. The lack of haptic information requires greater mental concentration from surgeons to complete a task, causing him to slow down the gestures and wait for visual cues that indicate the level of force applied or the type of tissue [74] [96].

Whether force feedback increases or not the surgical precision and outcome in MIS robotic procedures is still under debate [105] [113] [34], but recent studies confirm that the haptic

feedback can increase the performances in tissue discrimination [98] and can reduce tissue damage [105] and surgical task duration [14].

A number of studies have been performed to determine the need for haptic feedback [98] [23] [47] [32] [10]. These studies show that the benefit of force feedback is very much task, user, and system dependent. Situations in which force sensing has been shown to be significant include microsurgery [87] [53], knot tying [10] [48] [76], palpation [11] [102], needle insertions [3], where knowledge of the insertion forces can improve needle placement.

Most of the robotic devices for MIS or needle insertions do not provide any force feedback and the outer control loop between the operator and the robot relies only on surgeon handâĂŞ-eye coordination. Since robotic systems become more complex and costly with the introduction of force sensing capabilities, haptic feedback is still an issue in commercially available surgical systems and no commercial robotic device has compelling force feedback to provide information about environment mechanical properties. Thus, the need for force sensing must be fully justified.

For instance, the famous da Vinci® surgical system is increasingly being used in several applications [12] [64] [20] [62] and the need for haptic feedback in these applications is known in terms of lowering force [106] and increasing accuracy [38].

2.2 Force sensors design

The desire to measure forces in RMIS arises from the limitations imposed by minimally invasive access conditions. In order to display the forces to the hand of the operator, specific sensors need to be designed to sense the small interaction forces between the tissue and the surgical instrument [75].

Force sensors design and implementation is a balance between miniaturization, sterilization possibility, cost and equipment encumbrance [100] [75].

The first step in sensor design is the identification of the force sensor position. In order to understand where to sense the forces, it is necessary to consider the configuration of the medical instrument and the forces that act on it. Since there are many different points of contact with the environment, the placement of the sensors must be carefully optimized. Table 2.1 shows a detailed view of the possible places where forces can be sensed on a general surgical instrument.

A force sensor placed at the tip of the instrument has the best performance in the detection of the exact interaction forces, but it needs miniaturization, sterilizability, high insulation, modification and customization of the standard surgical tool; whereas a force sensor placed far from the instrument tip will not detect the exact tool-tissue interaction forces and it will also integrate mechanical force noise coming from the friction between mechanical interfaces and from the intrinsic inertia. Depending on the need for force sensing, it might also be necessary to measure the hand-tool interaction forces and not only the tissue/tool interaction.

The second step in force sensing design is the identification of what type of forces need to be measured. Full representation of the instrument interaction with the tissue can only be achieved by simultaneously measuring three orthogonal forces, three orthogonal moments, and the actuation force. However, fore some applications (e.g. needle insertion) sensing forces in only some of the Degrees of Freedom (DOFs) might be sufficient.

The third step for sensor design is the choice of the sensing technology. A wide number of force sensors were developed using different sensing principles: piezoresistive sensors, piezoelectric sensors, capacitive-based sensors, and optical sensors. Table 2.1 summarize each sensing principle advantages and limitations [100].

Sensor design must meet particular requirement when used in MIS: range and resolution, size, biocompatibility, sterizability, sealing, cost. Sensor resolution should be at least one order of magnitude less than the force difference that needs to be resolved [60]. In reference [73], it was shown that a resolution of 0.01 N was optimal for a force range of ± 2.5 N for needle driving tasks. Sensors placed inside the body must be small (in the millimeters range) [56] [13] and made of biocompatible materials (non-toxic, non-reactant with the body, not damageable by body fluids) [39]. They must be able to withstand a sterilization procedure. The most common sterilization methods include steam (autoclave), ethylene oxide, and gamma and electron beam irradiation [61]. In order to work in environments that are wet, sensors must be waterproof and/or sealed [56]. Finally, they must be inexpensive, especially if they are designed to be disposable.

Table 2.1: *Locations for force sensing, adapted from [100]*

Location	Advantages	Limitations
On or near the actuation mechanism	• Some information is readily available, no need for sterilization or miniaturization of additional sensing elements	• Affected by friction, mechanism play, backlash, gravity, and inertia within the instrument. • Sensing is taking place far away from where the forces are being applied. • Indirect force measurement can overestimate the grasping forces
On shaft outside entry port	• No constraint with respect to size. • Does not necessarily need to be sterilizable. • The information is useful for the design of robotic devices or in calculating the amount of force the hand needs to apply	• Measurements are affected by forces at the trocar, so they are not a good estimate of tool-tissue interaction forces
On the access channels	• Can measure interaction forces between the instrument and the tissue surrounding the instrument as it enters the body in order to minimize tissue damage	• Sensing elements have to be sterilizable and to work in warm and humid environments. • The size of the elements is limited to the size of the access channels
On shaft inside the body	• Able of measuring kinesthetic forces acting at the tip of the instrument	• Must be sterilizable and must work in warm and wet environments. • The size of the elements is also limited to the size of the port. • Affected by mechanism friction distal to the sensor placement
On tool tip	• Capable of measuring kinesthetic and tactile forces acting at the tip of the instrument. • Not affected by mechanism friction	• Must be sterilizable and must work in warm and wet environments. • Severe space limitations, as the size of the elements is limited to the tool tip

Table 2.2: *Force Sensing Techniques, adapted from [100]*

Technology	Advantages	Limitations
Strain gauges	Small size and can be sealed in a waterproof environment. Multi-axis measurement is easily achieved	Multi-axis measurement is easily achieved Sensitive to electromagnetic noise and temperature changes leading to drift and hysteresis. Tradeoff between the sensitivity of the measurement and the stiffness of the structure
Optical sensors	Forces can be measured in as many as six DOFs. They can be used inside magnetic resonance imaging (MRI) scanners. Also, they can detect changes with high sensitivity and reproducibility, and no hysteresis	Limitations include sensitivity to light intensity changes caused by bending of the cables or misalignment, and that optical fibres cannot typically achieve small bending radius
Measurement of actuator input	The system is no longer limited by the sensor bandwidth (which can make a control or feedback system unstable), and it is not necessary to incur the cost of force sensors. Does not rely on force sensors, which often do not operate properly when exposed to high temperatures and humidity	Very sensitive to uncertainties ; so if the system cannot be properly modelled (due to high joint friction, for example), the estimation error can be significant
Capacitive-based sensing	Limited hysteresis, better stability and increased sensitivity compared to strain gauges	They need more complex signal processing and are more expensive
Resonance-based sensing	High signal to noise ratio and digital processing is possible	They are affected by non-linearities and hysteresis
Piezoelectric sensing	Since these materials generate their own voltage, no additional power supply is needed. They have high bandwidth, high output force, compact size and high power density	They are very temperature dependent and subject to charge leakages. This results in a drifting signal when static forces are applied, thus making them suitable for the measurement of dynamic loads only

2.3 Force feedback strategies: telemanipulation and comanipulation

In RMIS, force display to the user can be achieved with two different types of robot architectures: telemanipulation, where the user is remotely maneuvering the device, or cooperative manipulation, where the user and the robot cooperatively move the surgical instrument (e.g. the needle).

Telemanipulation, with impedance control [34] [97] [26], allows performing surgery remotely and it is the most implemented platform for RMIS. Robots of the impedance type are backdrivable and have actuators to generate the force. In a linear impedance type device, the manipulator control (Figure 2.1) is designed not to track the trajectory alone, but rather to regulate the mechanical impedance of the manipulator. The relationship between the velocity ($\dot{X}$) and the applied force (F) is referred to as the mechanical impedance (Z_m). In the frequency domain is represented by

$$\frac{F(s)}{\dot{X}(s)} = Z_m(s) \tag{2.1}$$

and, in terms of position $X(s)$:

$$\frac{F(s)}{X(s)} = sZ_m(s) \tag{2.2}$$

Robots of the admittance-type are nonbackdrivable and have actuators which generate velocities. The nonbackdrivability typically comes from large friction and gearing in electromechanical systems. Mechanical admittance is defined as:

$$A(s) = \frac{\dot{X}(s)}{F(s)} \tag{2.3}$$

and is the inverse of impedance definition (2.1). The manipulator control (Figure 2.1) is designed such as the admittance matrix A relates the force error vector $E = F_D - F$ to the end-effector velocity perturbation, such as the command trajectory X_c is defined as

$$X_c = \int A(F_D - F)dt \tag{2.4}$$

To compare with impedance control, admittance control focuses more on desired force tracking control, and is more used in comanipulation tasks.

Abbott [1] described the complications of impedance control for telemanipulation in RMIS and how factors such as stiffness and damping of impedance force, sampling, and position measurement resolution effect the outcome. For telemanipulation systems, an operator would like a system as transparent as possible.

Transparency is defined as the ratio between transmitted and simulated impedance where the ideal ratio is unity for a desired bandwidth [55]. With the highest transparency, the operator would feel as he/she is interacting directly with the soft tissue. For a grasping task, sensing and display of all the seven DOFs of haptic information (three forces, three torques and grasping force) are needed [69] in addition to tactile information [103], in order to reach perfect transparency. There is a trade-off between stability and transparency [92] [37] and high force feedback gain can lead to instability and performance limitations [55]. Furthermore, asymmetry between the number of DOFs in force sensing and the number of DOFs in a haptic device can affect stability in bilateral teleoperation. Two examples of most advanced impedance type telemanipulation systems for surgery are the widespread da Vinci® platform, which is the actual reference standard for clinical RMIS and the DLR MIRO robotic system, a versatile and extensible lightweight robot platform that is expected to meet demands of various surgical applications, rather than a specific procedure [35].

Cooperative manipulation is not so widespread as the tele-manipulation approach. Comanipulation implies the simultaneously cooperative control of instruments by the surgeon and robot. The robot can implement safe constraints, filter human commands, compensate tools/robot weight, or have a more active behavior like active guidance and impedance. The definition of safe and forbidden zones restricts the tool motion, increasing safety. Compared to teleoperation, comanipulation brings together the accuracy of technology and the experience and dexterity of the surgeon. In this way the surgeon is still in charge but with augmented capabilities. Two commercial comanipulation system, the MAKO Surgical corp® system (Fort Lauderdale, FL, USA) [94] and the Acrobot® Active Constraint Robot (London, UK) [110], have shown superior outcomes relative to conventional surgery [21]. Aimed at knee replacement surgeries, these systems implement active constraints during the bone cutting process.

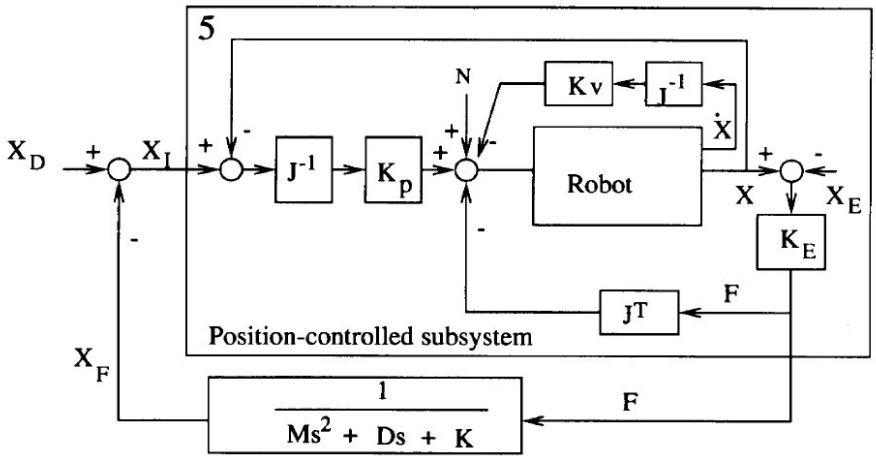

Figure 2.1: *Position based impedance control from [111]. J is the robot Jacobian matrix, X_D is the desired position vector in the task space, X and $\dot{X}$ are position and velocity vectors in the task space, X_E is the position vector of the contacted environment, K_E is the net stiffness of the sensors and environment, and F is the resulting contact force vector in the world space. K_p and K_v are the control gains, usually chosen as diagonal matrices. M, D and K are the desired inertia, damping and stiffness values respectively*

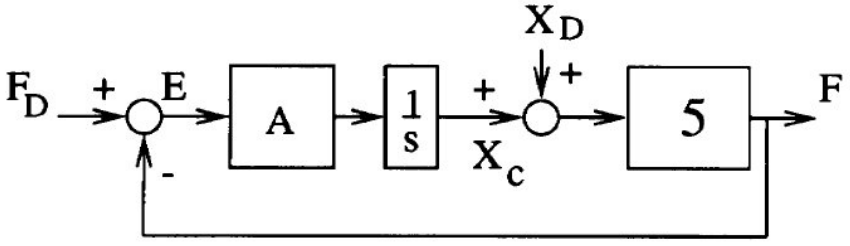

Figure 2.2: *Admittance control from [111]. The box with the number 5, is the same as shown in Figure 2.1*

.

Active constraints basically assert resistive forces to the surgeon hand in order to confine the procedure to a "safe" zone, which has not to be crossed. In neurosurgery, the ROSA^{TM} system (Medtech, Montpellier, France) uses comanipulation with haptic feedback for manual guidance of the robot close to the surgical tool entry point on the patient skull. Comanipulation with admittance control and force-to-motion scaling, showed high accuracy in highly demanding surgical procedure, like eye microsurgery [101] [84].

2.4 Clinical application: needle insertion procedures

Probably the largest sales of a commercial system for RMIS have been in the area of the manipulation of laparoscopes, but there is also an other clinical application where RMIS plays a role, when thin devices (needles or catheters) are inserted inside the tissue in order to perform diagnosis or treatment. In modern clinical practice, subcutaneous insertion of needles and catheters is one of the most common minimally invasive procedure. Common needle insertion application are blood sampling [114], biopsy [44] [16], brachytherapy [108], anaesthesia [99] and electrode placement for neurosurgery [80]. The complexity of such procedures is related to several elements, but we can consider the following factors to be the most relevant:

- *depth of the target to be reached inside the body*: the deeper is the position of the target inside the body the longer will be the path of the needle to reach the area of intervention. The longer the path, the higher is the risk to meet important critical structures that needs to be avoided.

- *location of the target inside the body*: the target can be placed inside vital and/or complex organs (such as the brain, the liver or the spine), which complicates the procedure and the planning of the needle path to be followed

- *lack of visual clue on the needle position during the advancement*: in most of the procedures, the operator cannot see the tip of the needle inside the body and must rely only on his experience

In these procedures, where the surgeon visual inspection is drastically reduced, the imaging misalignments, imaging deficiency, target displacement due to tissue deformation, needle deflection and target uncertainty are the main reasons for missing the target [81] [95] [41]. Also,

tactile information is lost because force feedback is filtered by the presence of the needle itself and the mechanical constraints of the access points.

Depending on the combinations of the previous elements, complications can arise. They have been studied in biopsy [5], brachytherapy [68] and in anaesthesia [9].

The knowledge of the needle insertion forces can give the surgeon better clues on the position of the needle inside the tissue, thus increasing safety [3]. In keyhole neurosurgical interventions (Figure 2.3), for example, where a straight needle is inserted from a small opening on the skull, the possibility to detect unexpected situations, like touching a vessel, could prevent vessel rupture (puncture) and consequently bleeding inside the brain parenchyma [52] [49].

The accuracy to be reached in needle insertions may vary depending on the application. In eye, brain and ear procedures common accuracy is in the sub-millimiter region, while placement accuracy for other region of the body (liver, prostate...) in millimiter scale is satisfactory (for biopsy, brachytherapy and anesthesia).

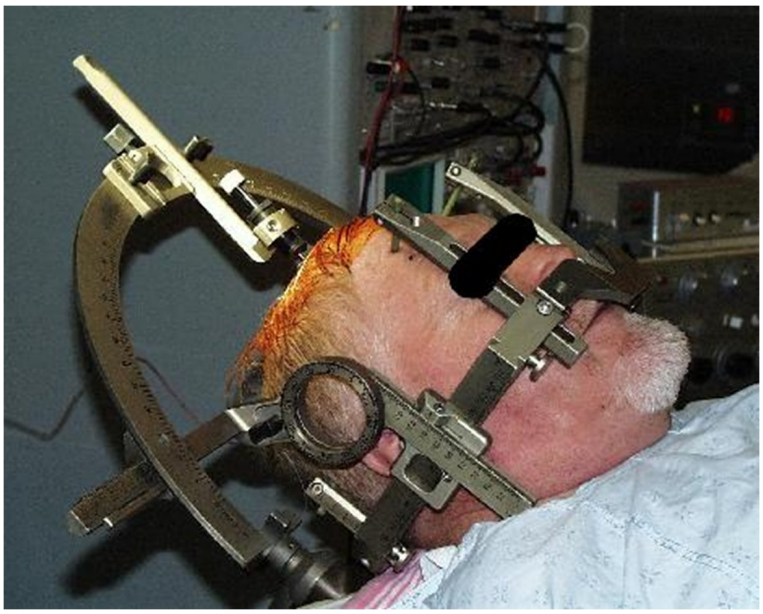

Figure 2.3: *Keyhole neurosurgical intervention. A straight needle is inserted by means of a small opening on the skull. Needle positioning and target reaching is achieved thanks to a stereotactic frame which helps the surgeon to replicate a path planned on the preoperative medical images.*

2.5 Project objective and thesis outline

The goal of the thesis is to improve surgeon performances during MIS, adding force feedback information during needle insertion procedure, focusing on neurosurgical interventions. The thesis is organized in two main chapters. The first part of the work was realized at the NearLab, Politecnico di Milano, Italy, within the European research project ROBOt and sensors integration for Computer Assisted Surgery and Therapy (ROBOCAST) FP7-ICT-2007-215190 and was aimed at investigating force sensing modalities to detect the small interaction forces between the needle and the brain tissue, in order to display them through an haptic interface on the hand of the surgeon in a telemanipulation scenario. Sensors were included in a small linear actuation device, realized in collaboration with the Medical Robotics Lab at the Technion, Israel Institute of Technology (Israel). Sensors were not directly placed on the needles, avoiding any sterilization issues. A new sensor-free force estimation was designed and performances compared to actual force sensing. Force display and control loop were realized in collaboration with the Sirs Lab at the University of Siena, using an Omega (Force Dimension, Switzerland) haptic interface, able to reproduce on the hand of the operator the sensed forces. My personal contribution was related to the design, optimization and implementation of the sensors, of the electronics and low level control algorithm for the piezo actuated linear driver, to the optimization of the master-slave outer control loop and to the experimental data acquisition and analysis.

The second part of this work was implemented at the Haptics Labs at the Johns Hopkins University in Baltimore, MD, USA and involved also the collaboration with the Surgical Assist Technology Group of the AIST Institute (Tsukuba, Ibaraki, Japan). The goal was to enhance force perception during needle insertions, giving to the surgeon the possibility to better feel the presence of discontinuities within the tissue (like membranes). The use of a coaxial needle allowed the possibility to separately sense the forces at the tip of the needle and the forces along the shaft, even if the sensors are not directly placed on the needle tip/shaft. The sensed force are then enhanced and fed back to the operator using a robotic assistant in a comanipulation approach, where operator and robot share the control. The system proved to be able to increase detection of thin membranes inside soft material, thus increasing the safety of the procedure.

My personal contribution was related to the optimization of the sensors, to the design, analysis and implementation of the force control algorithm for the coaxial needle insertion assistant, and to the human subject experimental data acquisition and analysis.

CHAPTER 3

Force sensing and display during needle insertion in keyhole neurosurgical interventions (telemanipulation)

During keyhole neurosurgery, small probes or electrodes are inserted with high accuracy in the brain through a small aperture in the skull (e.g. for biopsy, deep brain stimulation, stereo-EEG). Robotic systems can help such insertion with passive, active or semi-active operation. The former devices autonomously move to a predefined position (e.g. the probe's entrance pose) before locking and powering off. Examples are the Neuromate (Renishaw ltd., UK) and the ROSA^{TM}(MedTech, France), which replace the stereotactic frame in conventional neurosurgery [17]. Two active commercial devices, the NeuroDrive^{TM} and the Alpha-Drive (Alpha-Omega, Nazareth, Israel) provide for surgical electrodes insertion for brain signal recording. Semi-active robotic systems complement the surgeon action, rather than replacing it, and can be

tele-operated, i.e. the surgeon interacts with the remote slave robot through a master handling device [93].

Force feedback is helpful during surgical needle advancement to detect local mechanical properties of the tissue and to distinguish between expected and abnormal resistance for example, due to the unexpected presence of vessels. Transparency quantifies the fidelity with which the brain tissue properties are presented to and perceived by the operator [91]. From the master side, transparency is related to the mechanical characteristics of the haptic interface [104] and is quantified in terms of match between the impedance of the explored environment and the impedance transmitted to the operator [58], while for the slave side transparency is related to the accuracy in the force measurement.

Devices for force measurement can be implemented by putting sensors on the actuator, on the instrument shaft or on the instrument tip [75]. For example, in the LANS system [83], designed for performing biopsies and other neurosurgical interventions, a load cell is placed on the actuator, off-axis with respect to the tool. Integrating force sensors in-axis with the tip of a surgical tool is difficult due to the constraints on size, geometry, biocompatibility and sterilisability. Several attempts were made to put sensors on grippers or on dexterous instruments for laparoscopy [105] [51] and systems were designed for measuring forces of pulsating microvessels [19], but all these solutions are not actually suited for keyhole neurosurgery because of the size constraints.

Force feedback can be carried out also without the use of force sensors, through the position-position control where the difference between the nominal and actual position of the slave robot allows estimating the resistance forces being exerted by the environment [36] [54]. In [82], the authors present a force feedback system where the position error is detected and reflected as force to the master hand control. Results on accuracy in force measurement are not reported. If an accurate dynamic model of the actuator is known, accurate environment force estimates can be obtained [91] [33] [45]. Control-based force estimation methods have clear advantages in terms of miniaturization and sterilization. It was also demonstrated [18] that the insertion force depends on the insertion velocity. Lateral vibratory actuation showed instead a decrease greater than 70% in insertion force during skin penetration [109].

In this framework, we evaluated the ability of a slave tele-operation system prototype, part

of the ROBOCAST system [65], for biopsy probe insertion in estimating, with two methods, the resistance to the advancement (force) experienced by a standard probe for brain biopsies within a brain-like material. The biopsy probe is inserted by a piezoelectric actuated inchworm device that can be driven by the surgeon through an Omega haptic device (Force Dimension, CH). The system was tested using different gelatine samples, mimicking brain tissue and at different velocities for both proposed methods. The objective of the study was to allow the neurosurgeon detecting the interfaces between tissues with different mechanical impedance (e.g. due to the presence of membranes or to vessels walls) in order to stop the procedure if an unsafe situation was encountered. The force resolution for this task should match or exceed human sensing resolution (Just Noticeable Difference (JND)), which is around 7% [43] [72] or human perception [28].

3.1 Miniaturized linear driver

Figure 3.1: *The ROBOCAST system in the operating room. The operator remotely operates an haptic interface (Omega3, Force Dimension, CH) in order to introduce straight needles inside the brain for tissue sampling or for electrode placement. The needle is driven by a rigid probe driver which is attached to a kinematic chain constituted by three robots (13 DOFs).*

A miniaturized probe driver was realized at the Medical Robotics Laboratory of the Technion Israel Institute of technology within the framework of the ROBOCAST project. ROBOCAST combines navigated and robotic approaches (Figure 3.1) to address minimally invasive

neurosurgery procedures (e.g. biopsy) through a small aperture in the skull (keyhole neurosurgery). The system envisages a Human Computer Interface (HCI), with an intelligent context-sensitive communication and an haptic-driven capability, a multiple-robot chain with redundant degrees of freedom and a hierarchical structure, an intelligent autonomous trajectory planner, a high level controller and a set of field sensors. The mechatronic design consists of a modular robot (a kinematic chain composed of three robots totaling 13 DOFs)) holding the instruments for the surgeon and inserting them in the brain with a smooth and precise feedback controlled autonomous movement. The framework is designed for intervention of brain biopsies or electrode insertion, where straight needles are inserted into the brain. System accuracy and safety are extended by means of different sensors: an active marker optical tracking system, NDI Optotrak Certus (NDI Inc., Ontario, Canada) which surveys the overall robotic chain; an electromagnetic tracking system, NDI Aurora (NDI Inc., Ontario, Canada); and an ultrasound imaging device, Prosound Alpha 7 (Aloka Co., Ltd., Japan). Robotic actuators are:

- the Gross Positioner (GP) (PathFinder, Prosurgics ldt, UK): a serial 6 DOFs arm [22];
- the Fine Positioner (FP) (SpineAssist, Mazor, Israel): a parallel 6 DOFs Parallel Kinematic Machine, used to further correct the targeting [90];
- the Linear Actuator (LA): 1 DoF piezo-actuator, which advances the biopsy linear probes and whose performances are analyzed in this chapter.

The GP is a serial robot and thus it has a large workspace (about a sphere of 1 m of radius) with a low accuracy (0.5 mm [27]), while the FP has a small workspace (about a cube of 40 mm of radius) with high accuracy (0.1 mm). In the ROBOCAST framework, the GP is thus used to make the rough placement of the surgical tool on the desired entry point on the skull, while the FP is used to improve the positioning accuracy with fine movements. An haptic device (Omega3, Force Dimension, Switzerland), a 3 DOFs device, is used by the surgeon to move the straight probe frontward and backward through the LA.

In Figure 3.1 the intra-operative scenario is shown.

The Linear Actuator (LA) is an inchworm type piezoelectric (Figure 3.2), with two clamps, the Back Clamp (BC) and the Forward Clamp (FC), and one Pushing element (P). BC, FC

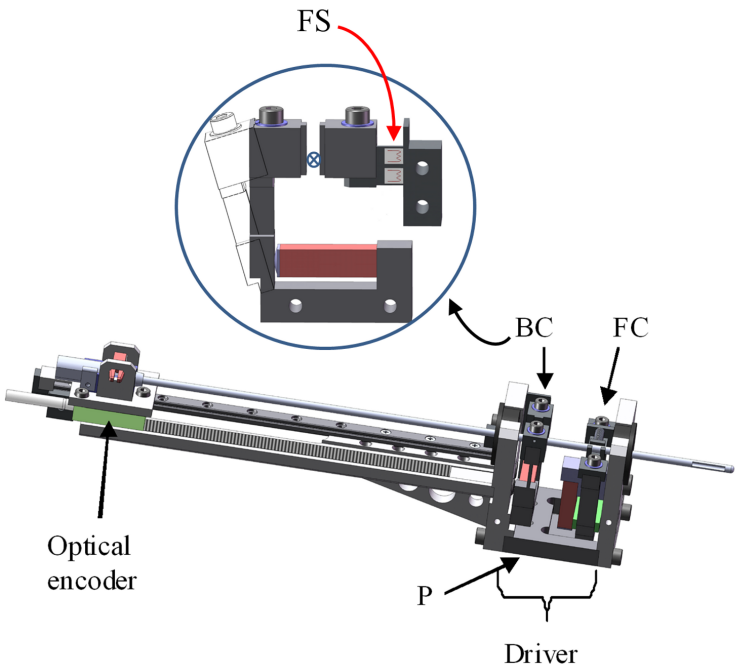

Figure 3.2: *Slave linear driver of the ROBOCAST system [65]. It encompasses: 1) a linear piezoelectric actuator, with an inchworm piezo-actuated motor with two clamps, the Back Clamp (BC) and the Forward Clamp (FC) and one extension element, the Pushing element (P); 2) a linear optical encoder; 3) a Force Sensor (FS) glued on the BC element.*

and P are actuated by 3 multilayer piezoelectric devices (Noliac, DK). In order to increase the piezoelement stroke, mechanical amplifiers were used in the BC, the FC and the P element (Figure 3.3). The clamping device BC is stationary and fixed on the support frame, while the FC is mobile and it is mounted on the P element. The surgical probe is hold by the clamping devices (Figure 3.3). The resulting needle motion is a micrometric step advancements, resembling the motion of an inchworm (Figure 3.4). The velocity is regulated by the voltage applied on the P from 8 to 32V (23.4mV step-size), since the variation in voltage changes the piezoelement stroke amplitude. The actuator is equipped with an optical encoder (LIK 41, Numerik Jena, Germany). The LA allows backward and forward motion of the needle. Two different cycles of opening, closing and pushing were implemented for the two types of motion: the stroke sequences for the forward and backward motion are reported in Figure 3.4 and the corresponding activations of BC, FC and P are reported in Figure 3.5 . The frequency of step actuation is 100Hz (10ms per motion cycle). In order to make the probe advance, the needed mechanical steps are six (Figure 3.4).

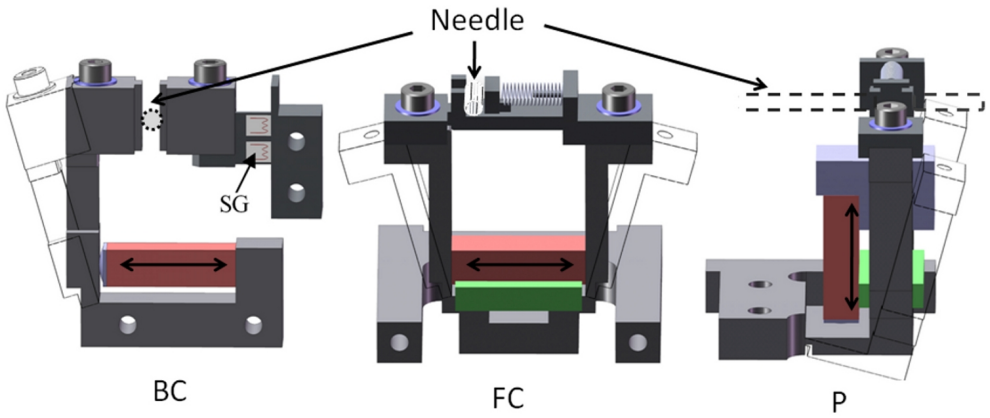

Figure 3.3: *Mechanical amplifier for BC (on the left), for the FC (in the middle) and for the P element (on the right). On the BC, the SG position is shown. The red blocks are the piezo-elements*

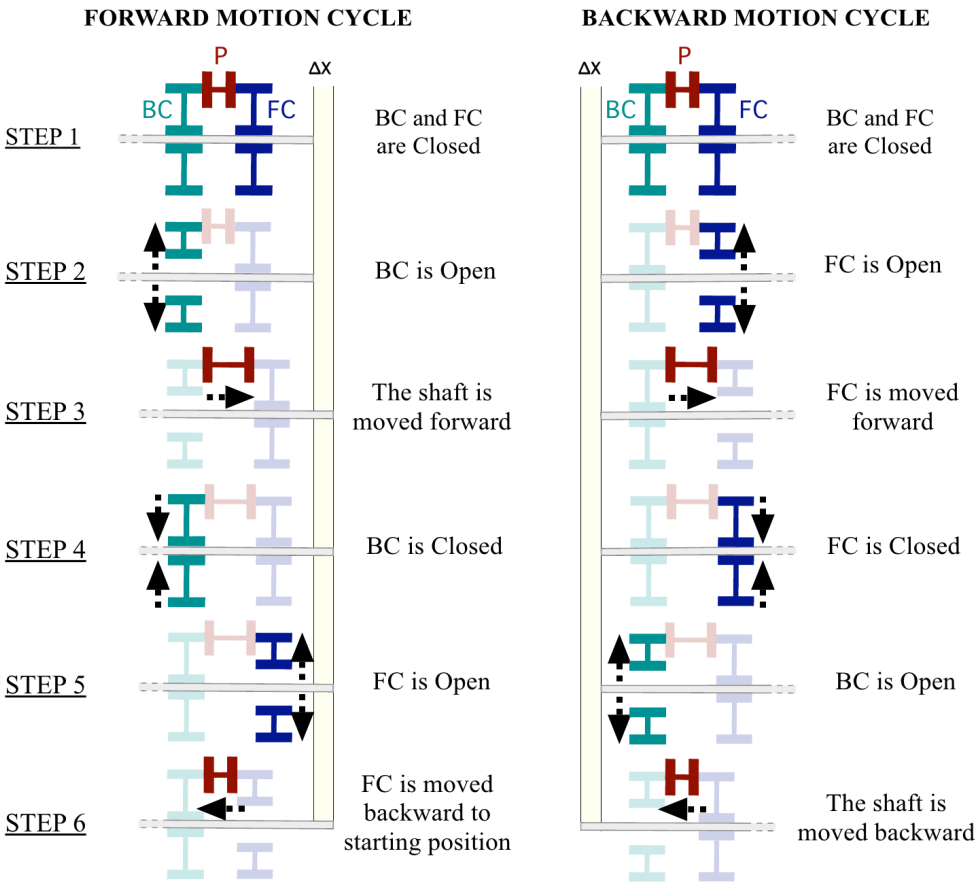

Figure 3.4: *Forward and backword cycles of the inchworm actuator*

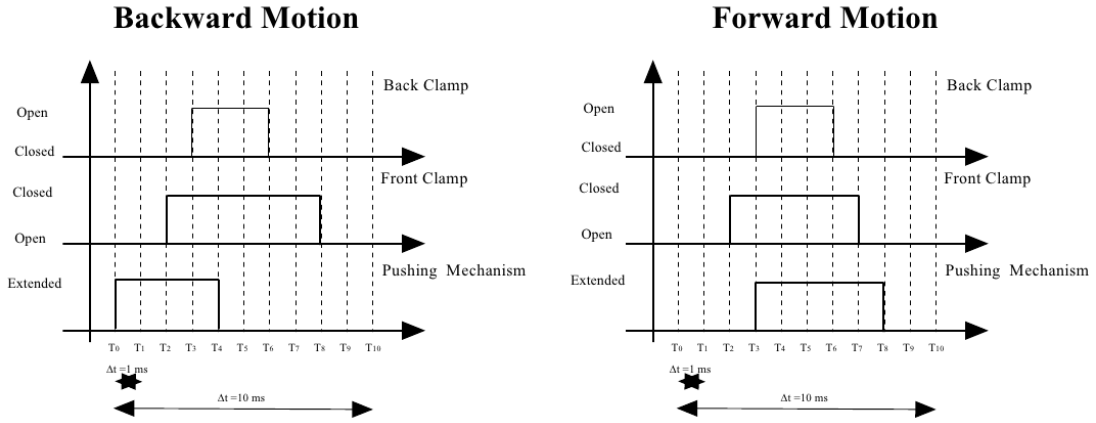

Figure 3.5: *Timing of the piezo driving commands that activates the BC, FC and the P for forward and backward motion.*

A Proportional Controller (PC), with gain K_p, was designed in order for the slave end-effector to track the master end-effector. The control scheme for the tele-operation system is represented in Figure 3.6. The X_{surg} position, input by the user to the Omega system, is rendered as X_m and then scaled times K_x for defining the nominal probe tip position X_{Sm}. X_s is the actual tip position. V_{cmd} is the nominal velocity, obtained by multiplying the position error (X_{Sm}- X_s) times K_p gain, that was tuned to be 70. This value allowed obtaining a wide bandwidth of the controller and avoiding permanent saturation of the non-linear function f, which states the relationship between the nominal velocity (V_{cmd}) and the input command ($U_{in} = f(V_{cmd})$) and was experimentally determined.

3.2 Force sensing strategies

The resistance force experienced by the probe (f_{PROBE}) during the insertion in the tissue is:

$$f_{PROBE} = f_{CLAMPING} + f_{ENVIRONMENT} + f_{HYDROSTATIC} \tag{3.1}$$

where:

1. $f_{CLAMPING}$ is the friction due to the machining tolerances of the surgical instrument conflicting with the clamps of the LA,

2. the push of the displaced gelatine ($f_{HYDROSTATIC}$) cannot overcome 0.78mN and there-

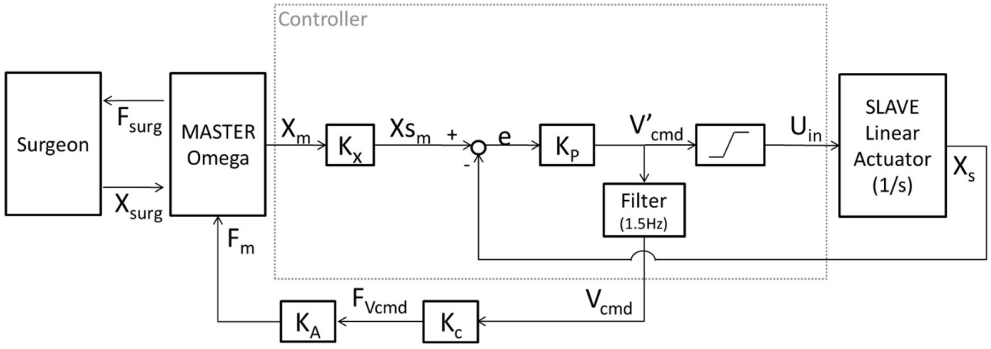

Figure 3.6: *Control scheme: the surgeon input X_{surg} is translated into the reference position signal X_m, which is then multiplied times K_x (10). The error between the reference position signal X_{sm} and the actual position X_s (measured by the linear encoder) is multiplied times the proportional coefficient of the controller (K_p). The resulting signal is converted into a voltage control signal ($U_{in} = 9.11V_{cmd} + 1.47$, U_{in} bounded between 8 and $32V$, saturated below and above this interval) and input to the LA controller. The force estimated valued (V_{cmd}) is then multiplied for a calibration value (K_C), obtaining the force value (F_{Vcmd}), and then amplified ($K_A = 2$) and cast back to the surgeon (F_{surg}).*

fore can be disregarded,

3. $f_{ENVIRONMENT}$ is the actual brain resistance force (cutting force plus friction force).

The resistance force experienced by the probe (f_{PROBE}) was measured:

1. by using a calibrated Force Sensor (FS);

2. by the estimate provided by filtering the nominal velocity signal, F_{Vcmd}, which in turn is proportional to the difference between the nominal and actual tip position (X_{Sm} and X_S as shown in Figure 3.6).

3.2.1 Force sensor design

The FS (Figure 3.7) is made of four Strain Gauges (SGs) ($4.1 \times 5.7mm$ - Vishay EA-06-031CE-350) glued on the BC element in full-bridge configuration, sensing resistance during the probe advancement (gauge factor 2.08, nominal resistance 350Ω, excitation voltage $10V$, amplified with bandwidth $0 - 1kHz$ and $gain = 250$).

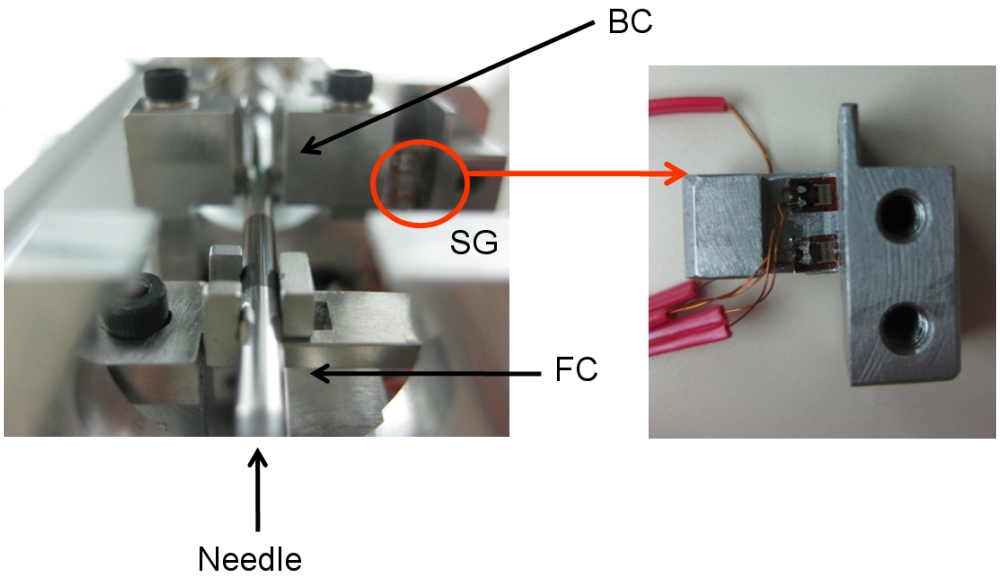

Figure 3.7: *Force sensor on the BC element of the LA. Four strain gauges were glued in a full bridge configuration on one of the two opening/closing parts of the clamp. The sensor is able to sense forces acting along the needle shaft*

3.2.2 Sensor-free design

Considering the control loop shown in Figure 3.6, we estimated the forces exchanged between the tissue and the needle:

1. filtering the nominal velocity command V'_{cmd} and obtaining the V_{cmd} value,

2. calibrating the V_{cmd} value with a multiplier, (K_C), in order to obtain the force values ($F_{V\,cmd}$).

Then we added the possibility to scale the estimated force value with a variable gain, K_A before casting it to the surgeon through the rendering of the Omega (F_{surg}).

3.3 Experimental design and setup

3.3.1 Brain tissue mimicking material

Gelatine was prepared as a brain tissue surrogate. It was mixed at a ratio of 8%, 12%, and 16% with water. Similar mixtures were proposed in the literature for similar studies [28], since the

insertion force of a surgical probe in them is similar to that observed in ex-vivo brain tissue [78]. A new gelatine sample was used for each test in order to avoid inhomogeneity due to old tracks.

3.3.2 Experimental protocol

A Backlund biopsy probe (Elekta AB, SE, outer diameter 2.1 mm) was inserted repeatedly into the gelatine samples. Forward motion was tested, with the LA in vertical position, as in neurosurgical interventions. In order to analyse $f_{CLAMPING}$, an experiment was also conducted inserting the probe in a viscous liquid with a damping factor grossly comparable to gelatine (dishwashing gel), where $f_{ENVIRONMENT} = 0$.

Tests required a reference signal for comparing quantitatively the force estimated with the two proposed methods with a ground truth. To this aim, a calibrated (R-square: 0.998) load cell (AB BOFORS KRK-2), with $5mN$ accuracy, was positioned under the gelatine box to measure reference signal (see Figure 3.8). Five speeds for needle insertion were tested: $0.5, 0.8, 1.1, 1.5$ and $2mm/s$. For each speed the following data were recorded with a sampling rate of 100Hz:

1. force signal from the Force Sensor (FS) (f_{FS})
2. force signal, from the load cell (f_{LC})
3. nominal probe velocity (V_{cmd}), from which F_{Vcmd} was computed
4. probe position, measured by the optical encoder (X_S).

This protocol was applied to four kind of samples: viscous gel and gelatine with 8%, 12% and 16% concentration. Five trials were recorded for each speed and sample. Details on the experiments are reported in Table 3.1.

The signal from the force sensor, f_{FS}, and F_{Vcmd} were both numerically processed with a low pass FIR filter (101 samples, $f_{cut} = 1.5Hz$, Kaiser window). For each velocity and each gelatine sample, the load cell reference signal, f_{LC}, was used for calibrating f_{FS} and F_{Vcmd}; i.e. the least square linear model that minimises the residual error between four out of the five trials and the reference signal (f_{LC}) was computed. The model was then applied to the fifth trial set and the residual errors with respect to the reference (f_{LC}) computed. In order to gather a statistic of the measurement, the process was repeated five time ($j = 1, 5$ in 3.2 and 3.3) for

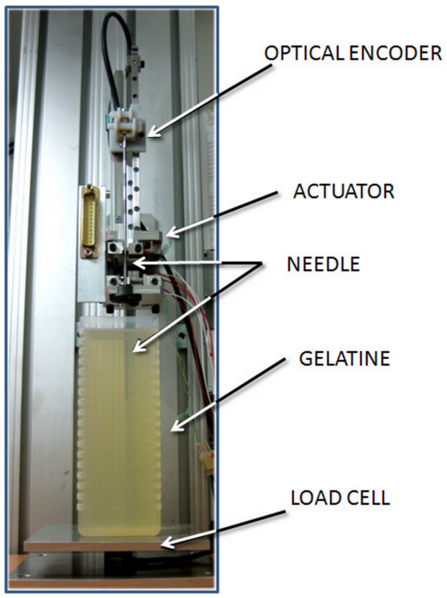

Figure 3.8: *Positioning of the load cell under the gelatine sample.*

Test performed	Number of trials N = 5
Sample	Dishwashing gel gelatine 8% gelatine 12% gelatine 16%
Nominal velocity	0.5 mm/s 0.8 mm/s 1.1 mm/s 1.5 mm/s 2 mm/s
Actuator position	Vertical
Stroke	60 mm

Table 3.1: *Description of the tests*

each condition always âĂIJleaving one trial outâĂİ of the five samples. The related Root Mean Square Error (RMSE) values were:

$$RMSE_{f_{FS}j} = \sqrt{\frac{1}{Q}\sum_{i=1}^{Q}(f_{FS_i} - f_{LC_i}) \qquad j = 1, ..., 5} \tag{3.2}$$

$$RMSE_{V_{cmd}j} = \sqrt{\frac{1}{M}\sum_{i=1}^{M}(F_{Vcmd_i} - f_{LC_i}) \qquad j = 1, ..., 5} \tag{3.3}$$

where Q and M are the number of samples in each of the five acquisitions. Since the acquisitions performed at the same needle speed had the same number of samples, the geometric mean of the RMSE values was computed and taken as performance evaluation figure for each speed. This was an overall assessment of the measurement fidelity along all the recordings. In order to focus on the evaluation of the dynamic behaviour, the slopes of signals (f_{FS} and F_{Vcmd}) during the fast phases of the trials were measured. Figure 3.9 shows a typical time course of the data where a puncturing phase (Phase 2), with the highest frequency content of all the recording, is easily recognised. The difference of the measurement obtained with the two methods (Δf_{FS} and ΔF_{Vcmd}), with respect to the reference load cell slope, was checked with the Kolmogorov-Smirnov test ($p < 0.05$).

3.4 Experimental results

Results metrics and relevance are summarized in Table 3.2.

Gelatine characterization Figure 3.10 shows the relationship between the environment force measured with the load cell (f_LC) versus depth (X_S), for each insertion velocity, after the probe punched the outer surface (phase 3 in figure 4). The signals represented are the means of the data acquired using the same concentration of gelatine at constant temperature parameterised with the insertion speed. The velocity-dependent effect is clearly visible in all the samples and increasing with concentration. Figure 3.11 shows the slopes of the linear model fitted (with maximum RMSE $0.0084N$, as reported in Table 3.3) to the force-position relationship, reported in Figure 3.10, vs. the insertion speed. The slope increases with the gelatine concentration (the viscosity coefficient increases). As shown, a good approximation to the function is provided by

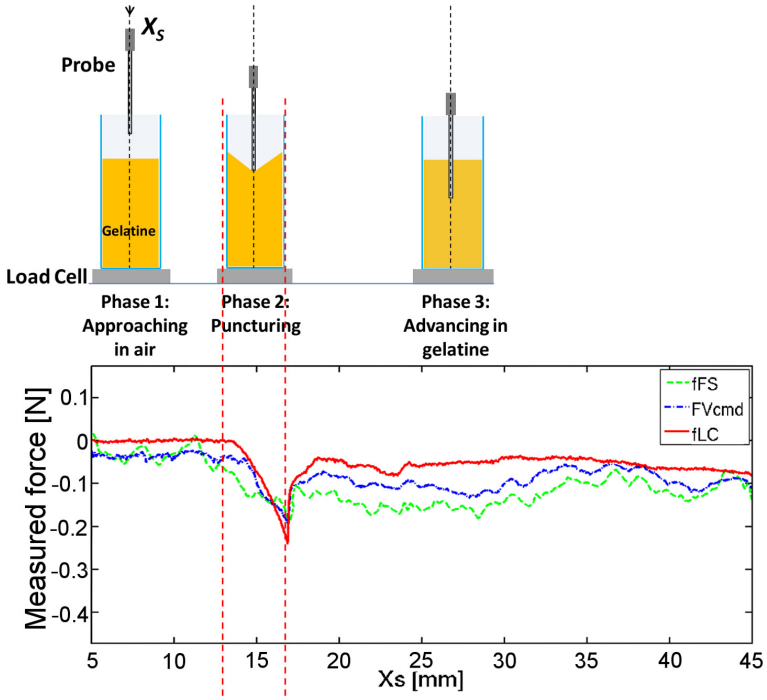

Figure 3.9: *Example of signals acquired during probe insertion (gelatine 12% at insertion velocity 0.8 mm/s).*

AIM	METRICS	RELEVANCE
Gelatine characterization	Force versus position/insertion velocity relationship	To characterize mechanical properties of the used material and compare results with literature
Clamping noise estimation	$f_{CLAMPING}$	To understand how results are influenced by the probe manufacturing
Accuracy of force estimation	RMSE of f_{FS} and F_{Vcmd}	To choose the better method for force estimation
Response to fast changes	Slope of the puncturing phase	To estimate ability to render force variation at interfaces

Table 3.2: *Results description*

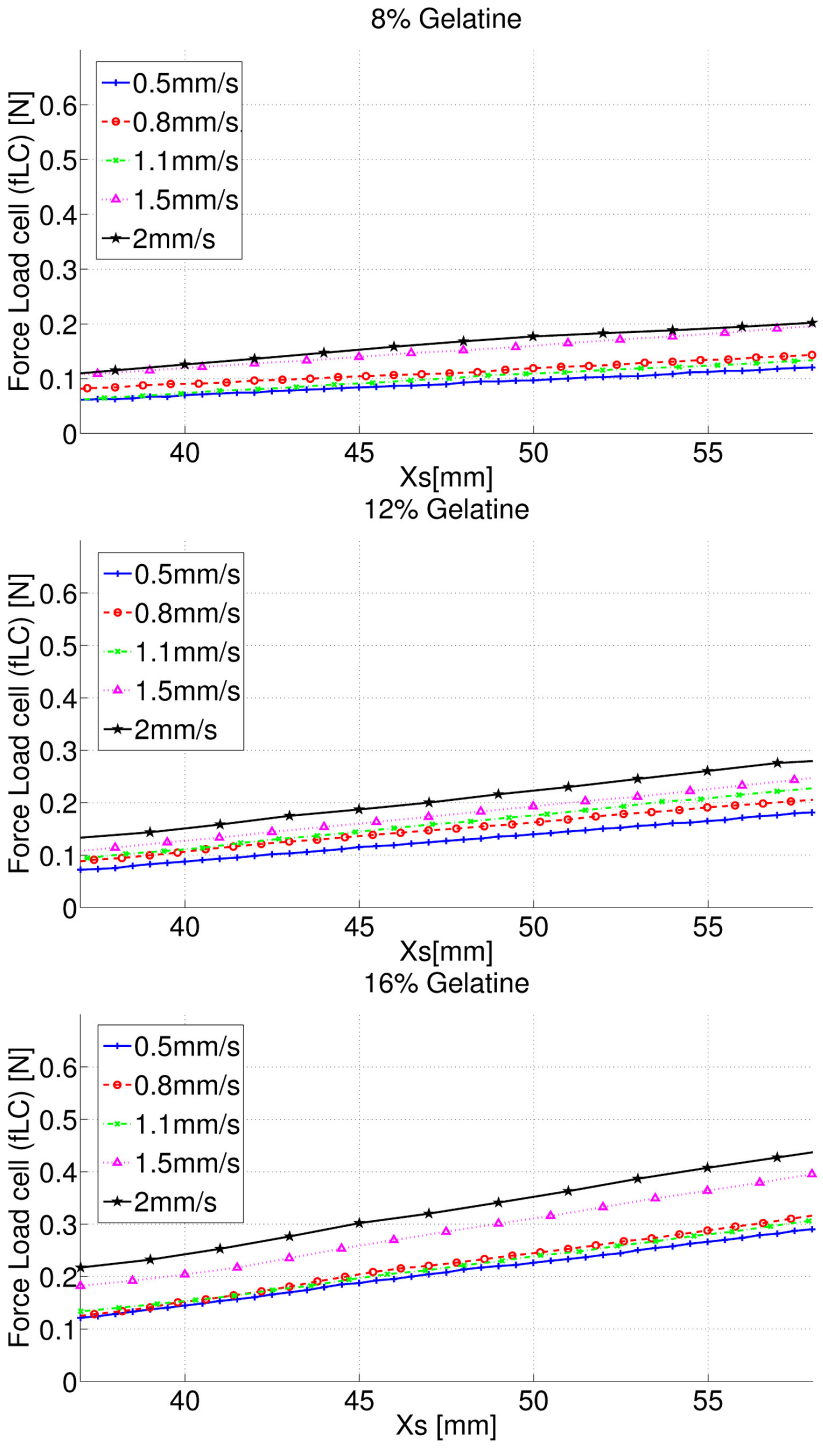

Figure 3.10: *Force (f_{LC}) vs. probe insertion depth for different insertion velocities. The mean values are reported.*

a scaled and shifted log curve for all the gelatine samples as already observed in [18].

VELOCITY	GELATINE 8% [N]	GELATINE 12% [N]	GELATINE 16% [N]
0.5 mm/s	0.0019	0.0017	0.0048
0.8 mm/s	0.0032	0.0034	0.0072
1.1 mm/s	0.0014	0.004	0.0049
1.5 mm/s	0.0032	0.003	0.0078
2 mm/s	0.0026	0.0064	0.0084

Table 3.3: *RMSE residual of the fitting of a linear model to the force-position relation*

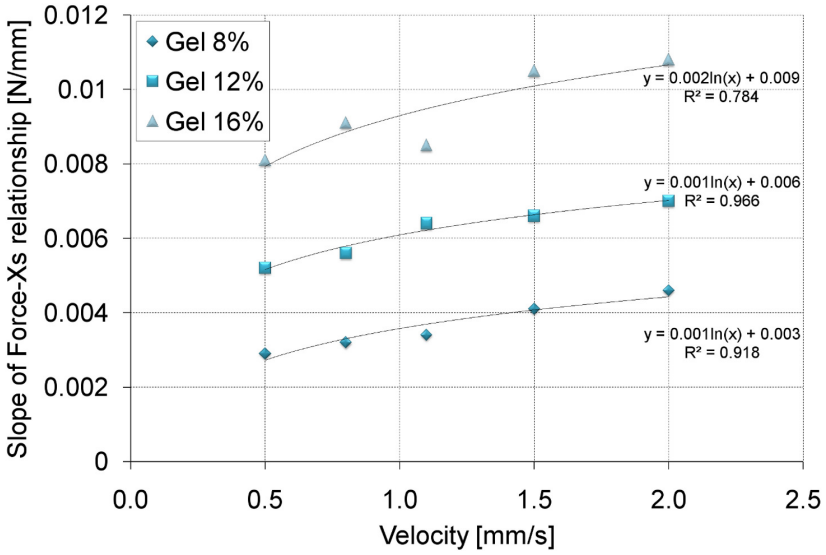

Figure 3.11: *Slope of the force (f_{LC}) vs. position linear model for different insertion speeds. The slope is computed fitting a linear model to the data of Figure 5 and then averaging across different trials. Solid lines represent the log best fit.*

Clamping force estimation Figure 3.12 shows fFS and F_{Vcmd} measured inserting the probe in a viscous dishwashing gel. The data have been normalised to their maximum value. Mean and standard deviation of the 5 trials performed at 1.5 mm/s speed are plotted. Clamping force $f_{CLAMPING}$ estimated from f_{FS} shows several peaks and troughs, due to the probe manufacturing imperfections, while F_{Vcmd} is clearly less affected by the probe imperfections (there is an offset of 0.01N during the whole probe advancement). During these measurements, f_{LC} was nil.

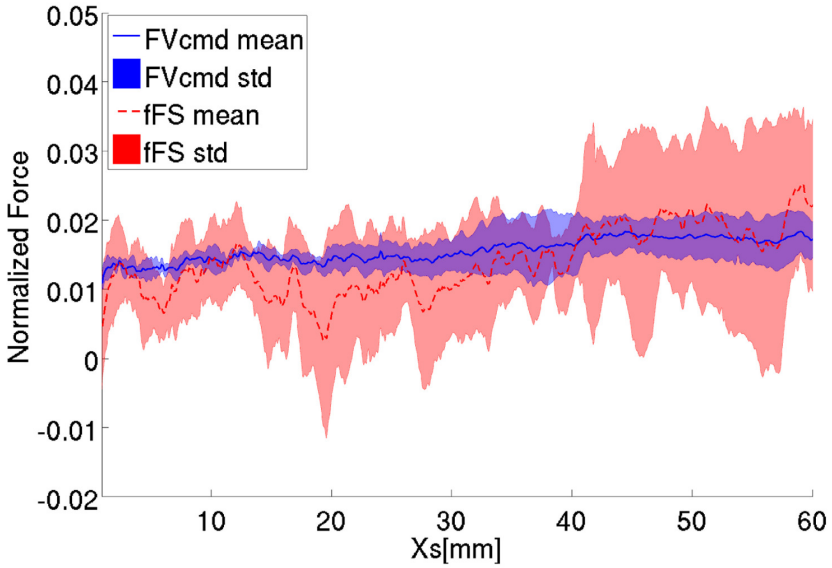

Figure 3.12: *Clamping force ($f_{CLAMPING}$) vs. probe insertion depth estimated by f_{LC} and F_{Vcmd} in the dishwashing gel at* 1.5 *mm/s.*

Accuracy of the resistance force estimation RMSE values of f_{FS} and F_{Vcmd} signals with respect to f_{LC} show comparable results, but the error does significantly increase with the gelatine concentration. Considering F_{Vcmd}, the gelatine 8% at 1.1 mm/s insertion velocity gave the best performances (RMSE less than 0.04 N). Maximum error was found with gelatine 16% at 1.5 mm/s (0.1 N). Since the experienced resistant force increases with speed as well, the increase in RMSE does not change the full-scale resolution as shown in Figure 3.13 where the RMSE values have been normalised on the maximum of the force measured in the trial. Similar results are obtained normalising with regards to puncturing force.

Response to fast force changes The fastest changes in force are experienced in Phase 2 of Figure 3.9. After the rupture of the outer membrane, the force reverts quickly close to the value measured in air and then starts linearly increasing due to cutting force and to the friction (Phase 3). Figure 3.14 shows the sensing performances at the puncturing phase, expressed as signals slopes difference, during Phase 2. ΔF_{Vcmd} is significantly lower than Δf_{FS} at 1.1 mm/s and decreases as the insertion speed increases.

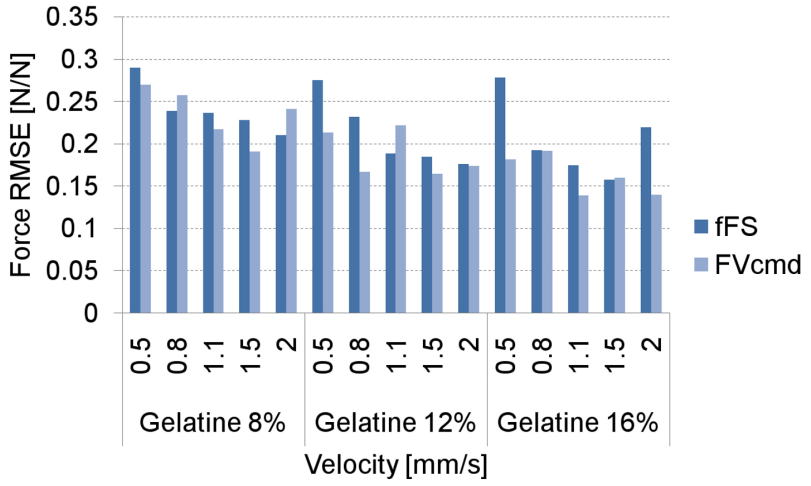

Figure 3.13: *RMSE values of both force sensor f_{FS} and F_{Vcmd} signals normalized with respect to the maximum force.*

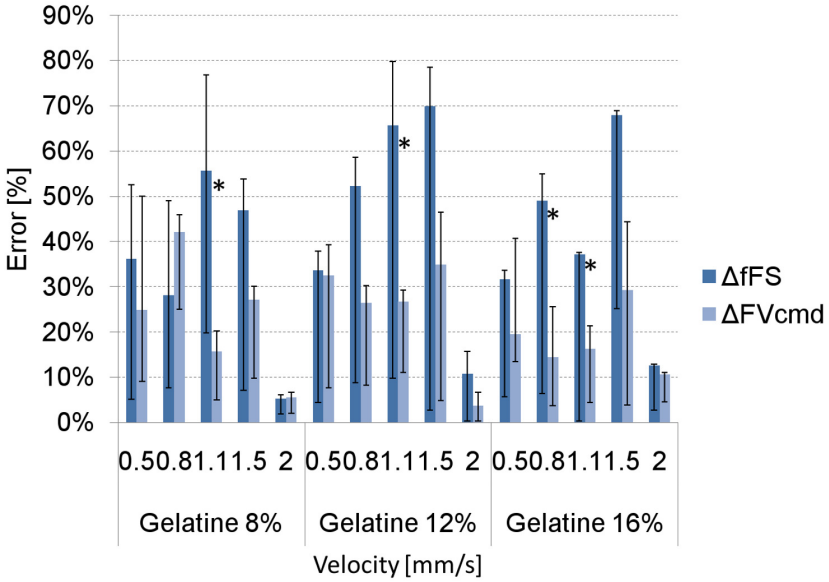

Figure 3.14: *Relative error during puncturing, measured as force signals slope difference with respect to the load cell (Median, 25^{th} and 75^{th} percentile).*

3.5 Sensor-free design improvement simulations

In order to improve the force estimation a new analysis was realized adding an integrator in the control loop ("Integrator" block in Figure 3.15 which connect V_{cmd} with ΔX_{env}). We simulated the control loop shown in Figure 3.15 in the Simulink framework (The Mathworks, Matlab R2008a) and we also e checked stability issues and system performances. Force estimate from the position error in the control loop of the teleoperated system were investigated starting from an accurate modeling of the whole Surgeon-Omega-Linear Actuator-Tissue system. The model scheme is reported in Figure 3.15. It includes the four models of all the systems acting in the haptic loop: the human model, the Omega device (master) model, the linear actuator (slave) model and the brain tissue model. The human model was obtained from [50] averaging the hand model parameters (mass, spring and damping); the master model was experimentally obtained; the slave device can be modeled as an integrator and the viscoelastic Zener model of the environment (brain tissue) was obtained according to [86]. The system was stressed with several step inputs (u in Figure 3.15). During such a input the brain model was also changed in order to test different tissue behaviors. This is accomplished changing the switch command signal (Switch cmd in Figure 3.15) from zero to one, in order to add or remove a brain tissue Zener model in parallel to a fixed one.

3.5.1 Simulation results

Results showed that the system is stable and able to accurately estimate the force steps as shown on the two bottom panels of Figure 3.16 where the estimated force with the position error is equal to the actual force on the tissue (red line, actual force, cyan line, estimated force). Adding the "integrator" block in the feedback loop allowed to have a better tracking of the constant force level in the steps. Without the integrator block the tracking of the constant force was decreasing with time. The force estimation with the position error is explained looking at the graphs of Figure 3.17, where the actual position of the probe tip differs from the theoretical position because of the resistance of the tissue. This difference is used to estimate the force acting on the tissue. Improvements should be investigated in order to reduce as much as possible the oscillation. However it is important to remember that such kind of input is impossible in a real

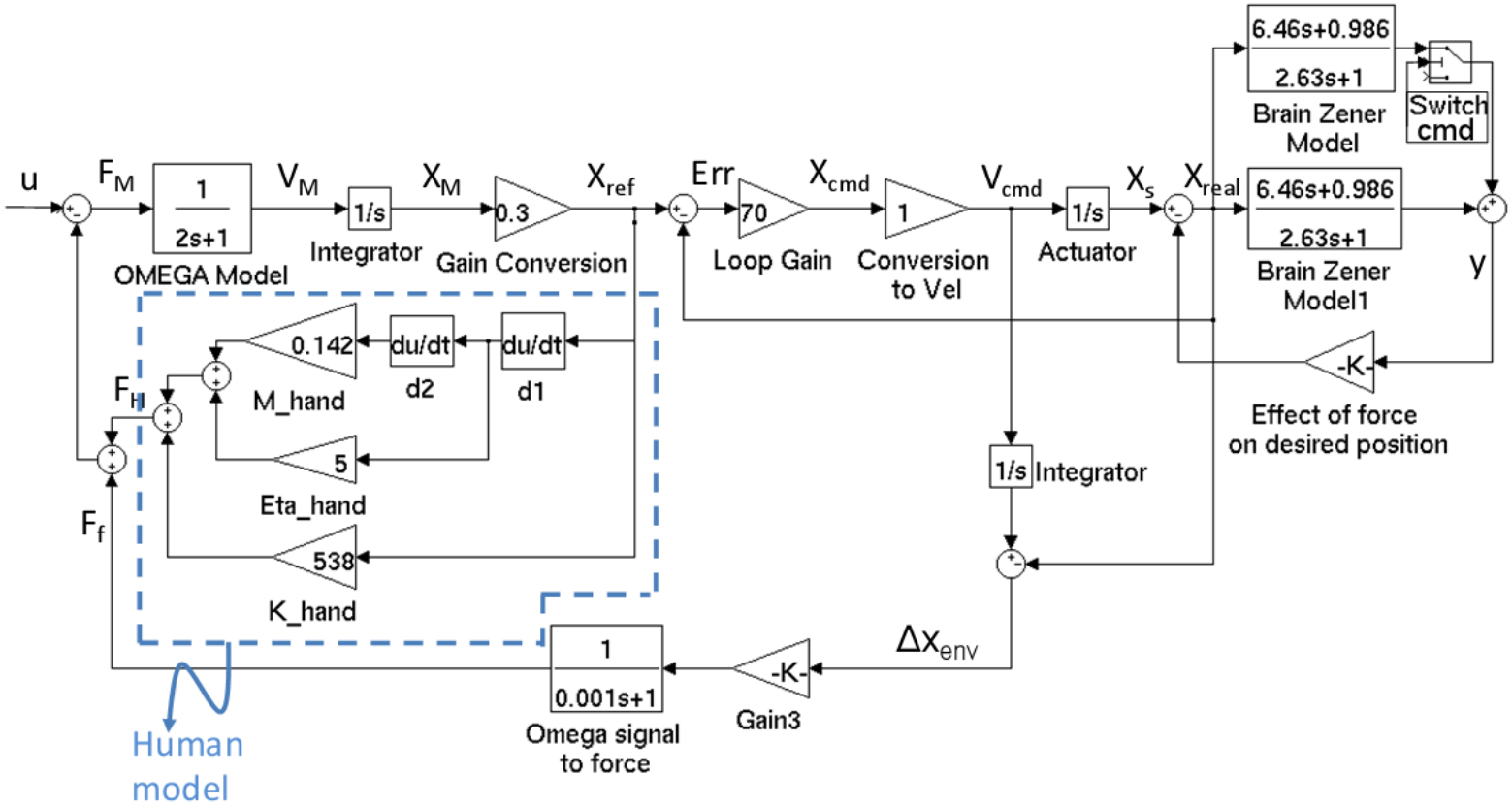

Figure 3.15: *Complete model of the haptic loop for the tele-operation of the surgical needle. The scheme takes into account the Human model [50], the Omega Model and the brain model obtained from the information in [86]. F_M is the force exerted on the master (Omega), V_M and X_M are the velocity and the position of the master, X_{ref} the scaled reference position, X_{cmd} is the position command wich is converted in velocity command V_{cmd} to the actuator, X_s is the actuator position without the effect of the brain tissue, X_{real} is the real position of the tip of the probe taking into account the environment behavior (Zener Brain model), ΔX_{env} is the position error for the estimation of the force, F_f is the force exerted by the Omega master device, based on the estimation provided by the position error, after being delayed considering the time needed by the device to convert the force signal to a real force (Omega signal to force block). M_hand, Eta_hand and K_hand are the human model parameters (mass, damping and spring) averaged from a previous work of Kuchenbecker et al. [50].*

scenario, since it is impossible for a surgeon to generate an ideal step input.

3.6 Discussion

In this chapter we described the experimental validation of a miniaturized tele-operated actuator for probe insertion in brain tissue, designed to provide the user with force feedback. In order to suit neurosurgical requirements, tip and shaft sensorization has been avoided for allowing easy sterilizability and the use of standard (not modified) surgical tools. Due to the small forces to be detected also off-axis sensors have been avoided since the moment generated acting on the bearing stresses the device friction forces hiding the signal. Furthermore one of the two measurement modalities (the position-position error) is sensor-less, in the sense that the deforming gage is the tissue itself.

In the experiments a phantom made of brain mimicking material was used, in order to test the system in controlled and repeatable conditions. Three different concentrations of gelatine in water were tested and the estimated forces were comparable with values reported in literature using in-vitro brain tissue [42] [88]. The most similar results with swine brain indentation experiments (maximum $f_{ENVIRONMENT}$ value 0.2N at 2mm/s insertion velocity) were obtained by using gelatine 8% . The gelatine 16% showed the biggest variance since its stability is the most temperature-dependent. To control this problem, the number of trials was kept limited (N = 5) to avoid changing of properties of the samples at room temperature. Further tests on the brain mimicking material behaviour are needed, in order to estimate tissue damage, but they were beyond the scope of this work.

Brain resistance force, $f_{ENVIRONMENT}$, was computed by filtering the signals coming from the force sensor and the input velocity command (V_{cmd}), proportional to the position error, which represented an estimate of the resistance force. Such estimates were both compared with the measurements of the load cell and resulted to behave almost in the same way, but the sensor-less sensing modality (F_{Vcmd}), beyond being immaterial, proved to be significantly better also during the puncturing phase, in correspondence of the interface crossing. Avoiding the need of any tip force sensor, the approach herein presented has clear advantages in terms of sterilization and miniaturization issues.

Due to the probe manufacturing (extrusion vs. rectification), the friction of the probe on

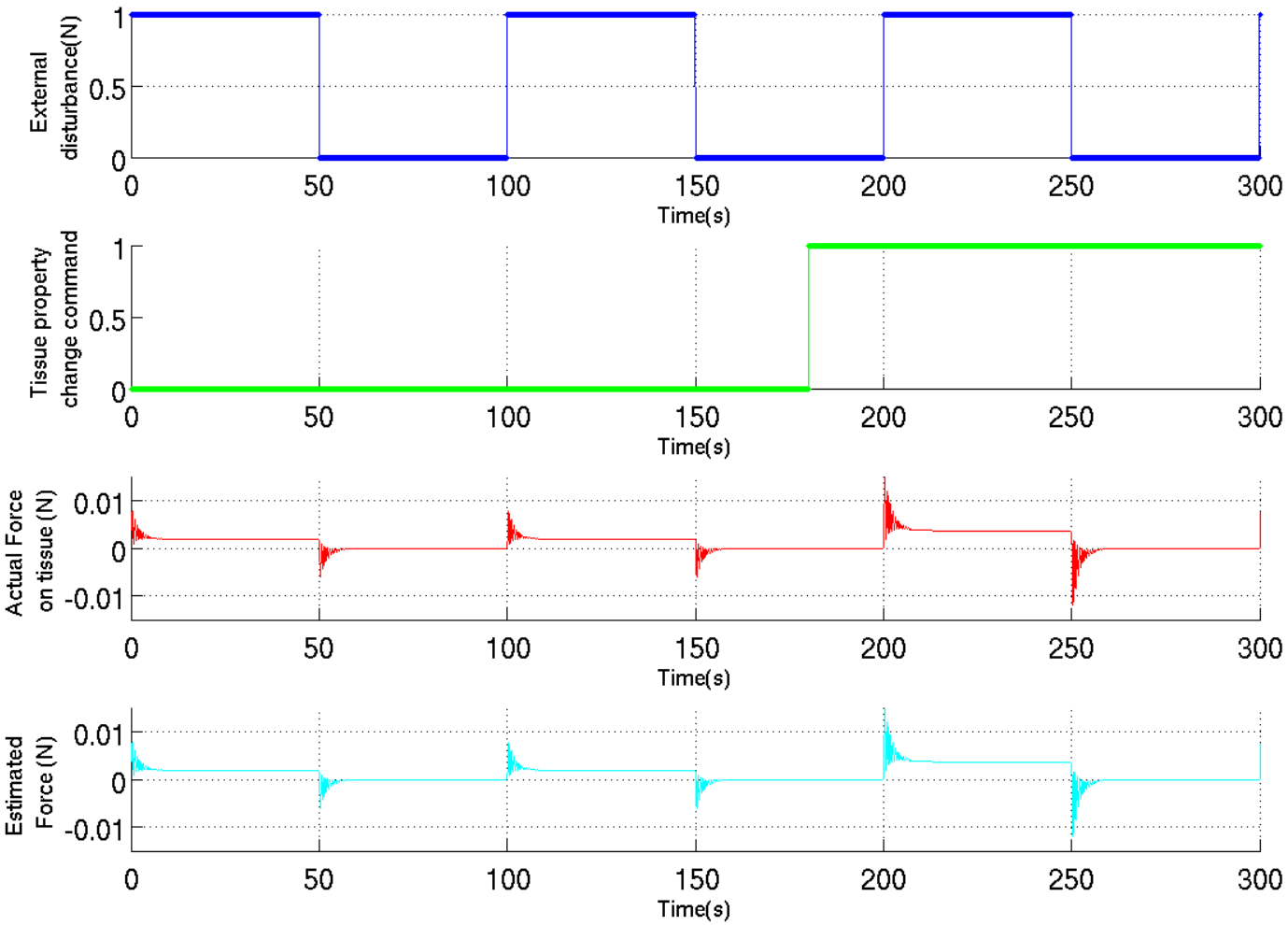

Figure 3.16: *The top panel shows the input force steps injected to stress the system. The first middle panel show command signal for changing the tissue model properties: when the signal change value form zero to one and viceversa another brain Zener model is added or removed, resulting in a changed environment behavior. The second middle panel shows the actual real force between the probe and the tissue. The bottom panel shows the estimated force from the position error. The system is stable and the force is well estimated (the change of the tissue model results in a change of the estimated force), following the actual force.*

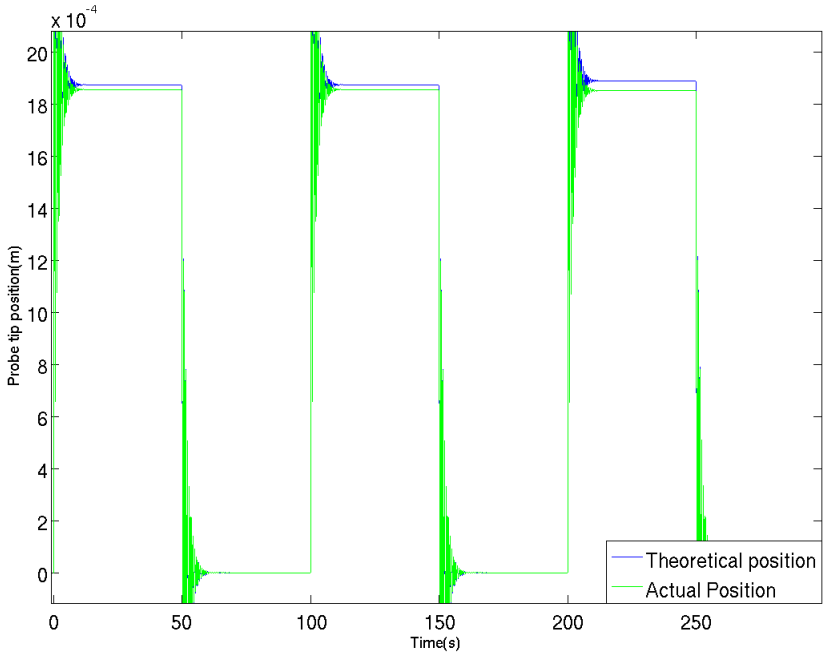

Figure 3.17: *Theoretical position and actual position of the probe tip for the same simulation showed in Figure 3.16*

the clamps, $f_{CLAMPING}$, can vary during the advancement, but the attempt to compensate it by gel measurements was unsuccessful. Also in this latter experiment, F_{Vcmd} showed to be the best estimator, for lower bias and scatter. System accuracy proved to potentially satisfy the neurosurgery application requirements since the maximum error was 0.16N as average value. Using the gelatine 8%, which proved to replicate brain tissue mechanical properties, the system resolution (worst case) is around 20% of the puncturing force, independently from the insertion velocity. That value even decreases in gelatine 16%. This result shows that the system can convey to the operator the information on tissue discontinuities with a Signal to Noise Ratio ($> 15dB$) close to the Just Noticeable Difference (JND) [43] [72] [89].

Previous studies report the effects of the tip shape and of needle diameter on soft human tissue [88] [3] and show that rotation of the needle significantly decreases the force required to advance in the tissue [40]. Also, an increase in needle insertion velocity could reduce the amount of tissue deformation [2]. The forward backward micro-vibrations (amplitude $6 - 10\mu m$, frequency $\sim 160Hz$), by-product of the inchworm-like actuator presented in this work, avoid sticking of the probe to the tissue as well. Also it allows increasing the velocity of each

single step at 8mm/s, limiting the total probe advancing velocity (2 mm/s maximum). The other great advantage of the inchworm-like actuator is its small size and weight compared with its long stroke of 120 mm (theoretically unbounded) and high position accuracy of $8\mu m$.

The proportional coefficient of the controller has been set as a trade-off between bandwidth ($f = K_p/2$) and the accuracy of estimation of $f_{ENVIRONMENT}$: for high proportional gain (K_p) values, the tracking error converges towards zero. Furthermore this parameter cannot be too high otherwise the nonlinearity of the voltage driver would turn the continuous controller into a relay (two values) controller. The stability of the control is guaranteed by the existence of only one real pole in the feedback loop. Furthermore, the control signal (U_{in}) saturates at 8 and 32 V, so the output variation is forcedly bounded. Further evaluation will be focused in the future on the tele-manipulation control, which was beyond the scope of this work. In particular the force feedback stability and accuracy during manual insertion will be taken into account considering the human operator in the control loop. Indeed, the controller pole frequency ($f = K_p/2 = 11Hz$) may allow the surgeon to introduce instability in the outer loop. The problem is avoided by the low pass filter at 1,5Hz cut off on F_{Vcmd}. Such low-pass filter also allows cancelling physiological tremor which has typical frequency content from 10 to 30Hz, and amplitude of $100\mu m$ RMS [79]. The delay caused by filtering satisfies the requirements of the application since it allows stopping the probe advancement within 1.3mm (at 1.1mm/s), if operator reaction time is 0.7ms, as reported in [34]. Real time implementation will lead to the use of an IIR filter requiring much less computational effort. Delay could also be reduced by playing with the bandwidth and the transition band.

The need for measuring the force feedback in tele-operation is proven: the surgeon feels more comfortable and confident and performances in terms of speed and accuracy are enhanced [34] [105]. The importance of tactile sensation in increasingly technical neurosurgical procedures makes accurate haptic feedback an important element also of simulation [59]. Due to its reduction of invasiveness, the possibility of using standard instrumentation, sterlizability (piezoelectric elements used can be sterilized in autoclave) and overall size, the system proposed is definitely suitable for neurosurgical applications. We also showed the capability to measure resistance without any additional sensors.

CHAPTER 4

Enhancing force sensing and display during needle insertion (comanipulation)

4.1 Introduction

In standard manual needle insertions, an operator introduces straight needles into soft tissues of the body for diagnosis (biopsy, blood sampling) and therapy delivery (drug delivery, electrode placement) [3]. In minimally invasive needle insertion, due to the limited access to the surgical site, the surgeon (or other clinician, such as an anaesthesiologist or interventional radiologist) cannot see the path of the needle inside the tissue and thus must rely on a limited sense of touch or an assumed needle path based on correspondence between the amount of insertion and pre-operative medical images.

The sense of touch is restricted in that the operator would like to feel the properties of tissues deep within the body, but the interaction with tissue is mediated by the needle. There is

no distributed tactile sensation, and force feedback is provided only at the base of the needle – which includes both tip and shaft forces. Sensing and displaying needle tip forces could give the surgeon better clues on the position of the needle inside the tissue [3] and allows more accurate identification of differences in soft tissue resistance (e.g., when hitting a vessel in the brain parenchyma during probe/electrode placement for deep brain stimulation). Improving position accuracy inside the tissue increases the operator's ability to precisely reach the target of the intervention, and identifying differences in tissue properties (e.g. subsurface structures as nerves) allows preventing unwanted tissue damage of vital structures along the needle path. Gerovich et al. [30] showed that real-time visual and force feedback improve the ability of users to detect puncture of different tissue layers during needle insertion.

A target application of this research is keyhole neurosurgical interventions, where a straight needle is inserted from a small opening on the skull down to the target inside the brain. In such procedures, vessel rupture (puncture) and subsequent bleeding inside the brain parenchyma is one of the critical aspect of the procedure with an incidence between 4% and 7% [31]. During the needle advancement, the possibility to detect unexpected situations, like a vessel on the needle trajectory, could prevent this highly dangerous situation, lowering the incidence of haemorrhagic complications inside the brain.

Most robotic devices for minimally invasive surgery and needle insertion do not provide any force feedback; the outer control loop between the operator and the robot relies only on surgeon hand–eye coordination [67] [70]. Whether force feedback improves surgical precision and outcomes in minimally invasive robotic procedures is under debate [105] [113] [34] [112], but recent studies confirm that haptic feedback can increase an operator's ability to discriminate between different tissues [98] and reduce tissue damage [106] and surgical task duration [14].

In order to sense interaction force between tissue and a surgical instrument, application-specific sensing techniques must be employed [75]. For needle insertion tasks in neurosurgery, small force variations at the needle tip are masked by the relatively large shear friction force between the needle shaft and the surrounding tissue. The design and implementation of force sensors for this application are challenging due to the constraints of size, cost, and equipment encumbrance [75] [100]. The position of the force sensor on the surgical tool/device plays a significant role. A force sensor placed at the tip of the instrument allows accurate detection

of the interaction forces, but miniaturization, sterilization, high insulation, modification and customization of the standard surgical tool are required. A force sensor placed far from the instrument tip is not subject to all these requirements, but does not accurately detect the tool-tissue interaction forces, since it integrates mechanical force noise coming from the friction between mechanical interfaces and device inertia [34] [75].

The interaction forces between the needle and the soft tissue, i.e. the friction force along the needle shaft and the poking/cutting force at the needle tip, were modeled in [25] [8] [4] [15] [46]. Such models were used in surgical simulators in order to improve the realism of virtual needle insertion for training and planning. Other models [71] [7] were used to improve detection of membrane puncture, by subtracting the modelled friction force from the total force sensed, thus enhancing detection of changes in tip force. Modelling errors, generated by the inhomogeneous tissue properties and by the force dependence on insertion speed, tissue properties, temperature and body fluid interaction, can corrupt the tip force estimation.

A different approach is presented in [107], where an instrumented coaxial needle was proposed to separately measure poking/cutting force at the needle tip and shear friction on the needle shaft using two different force sensors. A tissue model is not needed and the device reliably identifies the two force contributions since its performance is not influenced by modelling errors.

In this chapter we present a robotic assistant based on the coaxial needle scheme, with a cooperative manipulation architecture in which the robot and the surgeon simultaneously drive the surgical needle. Our purpose is to improve operator perception of small variation in tissue properties (e.g. crossing membranes inside the tissue) during needle insertion. Force sensors, placed far from the needle tip and shaft, allow separate sensing of the shaft and tip forces so the control algorithm can display only the latter to the operator. The effectiveness of the system was evaluated through an experiment with inexperienced users, who were asked to insert needles into artificial brain tissue and detect the presence of membranes.

4.2 Coaxial needle assistant

The device is equipped with a coaxial needle (Figure 4.1), in which an inner needle is inserted into an outer needle. The inner needle tip sticks out of the outer needle, thus the inner needle

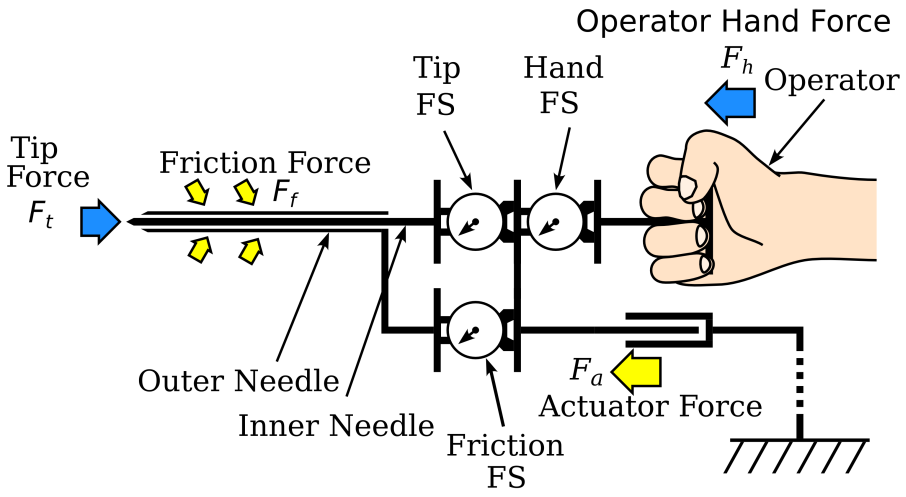

Figure 4.1: *Overview of the robotic coaxial needle insertion assistant. Three force sensors (FSs) are used to sense the total force applied by the operator (F_h), the force between the outer needle and the tissue (friction force, F_f) and the force applied by the inner needle to the tissue (tip force, F_t). An actuator drives the motion of the outer and inner needle together with the human operator.*

is not subject to friction force due to contact with the surrounding tissue. The two parts of the coaxial needle (inner and outer) are mounted on separate sliders, which are locked together, and they move along a linear guide. The inner needle slider is equipped with a handle for the operator to push it. The sliders are driven via a transmission cable by a geared DC motor (represented as the Actuator in Figure 4.1). It has one degree of freedom of linear motion along the needle axis, with 10 mm/s maximum velocity, 10 N maximum force and 130 mm stroke. The system specifications are summarized in Table 4.1.

Both the inner and the outer needles are inserted by the operator with the help of the actuator. The device is equipped with four custom force sensors (FS) sensing the inner needle poking/cutting (*tip force,* F_t), outer needle (*friction force,* F_f), operator (*hand force*, F_h), and actuator (F_a) forces, as shown in Figure 4.2. The operator force, F_h, balances the friction force, F_f, the tip force F_t and the actuator force F_a.

The force sensor coupled to the inner needle was designed with a full-scale range of 10 N, and the other sensors' full-scale ranges were both 40 N. The force sensors were calibrated with known forces obtained using weights (weight accuracy 20 μN, RMSE $=$ 4.2 mN F_t, 30 mN F_f, 72 mN F_h, 133 mN F_a). Each force sensor encompasses a flexure parallelogram mechanism with strain gauges connected as a Wheatstone bridge. Each bridge signal is amplified by instru-

Table 4.1: *Coaxial needle insertion assistant specifications*

Max velocity	10 mm/s
Max force	10 N
Overall stroke	130 mm
Motor type	Maxon DC Motor, 41.022.022-00.00-202
Voltage output control resolution	16 bit
Transmission type	cable
Optical encoder resolution	10 μm
Control update rate	5 kHz
Force sensor accuracy	F_t : 4.2 mN F_f : 30 mN F_h : 72 mN F_a : 133 mN
Force sensor resolution	16 bit

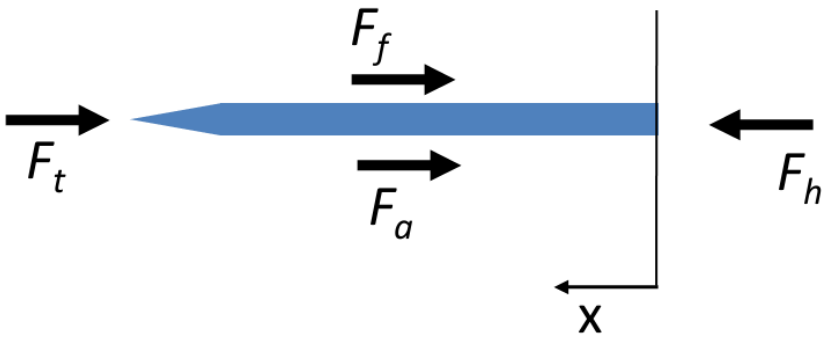

Figure 4.2: *Forces simultaneously acting on the coaxial needle: F_h is the force exerted by the operator hand, F_t is the force acting on the tip of the needle, F_f is the friction force between the needle and the surrounding tissue, F_a is the actuator force and x is the positive direction of motion.*

mentation amplifiers (INA118 and INA128, Texas Instruments). The coaxial needle position is measured by an optical linear encoder (LM-25CPMM-3S, Encoder Technology, 0.01mm resolution). The force signals, position signals, and control algorithm are acquired and updated on a computer at 5kHz with a real-time operating system (RT-Linux/GPL 3.2 rc1 with Linux kernel 2.4.29).

4.3 Comanipulation model analysis

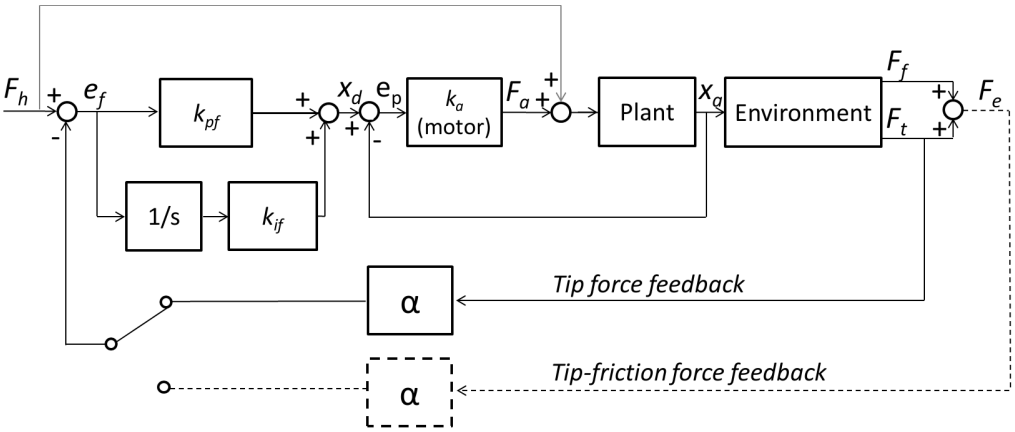

Figure 4.3: *Coaxial needle control scheme. F_h is the operator hand force, F_e is the needle-tissue interaction force measured by the force sensors (F_t and F_f), F_a is the actuator force, k_{if} and k_{pf} are the proportional and integral outer loop control gains, x_d is the desired position, $x_a$is the actual position, e_f is the force tracking error ($F_h - \alpha F_e$). The figure shows the two types of force feedback used: tip force feedback (solid line), where only the tip force is scaled by a gain, α, and fed back to the user; tip-friction force feedback (dotted line), where both the tip (F_t) and the friction force (F_f) are scaled and displayed to the user.*

The force-controlled actuator (Figure 4.3) amplifies the forces between the needle and the tissue and displays them to the operator. For this purpose, F_h is proportional to the tissue interaction force measured by the needle sensors (environment force) F_e, through a multiplier ($F_h \cong \alpha F_e$).

F_e can be set by the controller (Figure 4.3) equal to the force at the needle tip ($F_e = F_t$) or to the sum of the tip force and the friction force along the outer needle ($F_e = F_t + F_f$). Figure 4.3 shows the two types of force feedback that can be set in the control (*tip* force feedback and *tip-friction* force feedback).

An outer loop implicit force trajectory-tracking controller [85] was implemented to set the

desired needle position (x_d):

$$x_d(t) = k_{if} \int_0^t e_f(t)dt + k_{pf} e_f(t), \tag{4.1}$$

where $e_f = F_h - \alpha F_e$ and k_{if} and k_{pf} are the proportional and integral outer loop control gains [85]. The inner loop position-control is a proportional controller (k_a), which sets the actuator output F_a as:

$$F_a = k_a(x_d - x_a), \tag{4.2}$$

where x_a is the actual position. In this type of control, the position of the actuator (x_d) is set to minimize the error between the measured and amplified environment force (αF_e) and desired hand forces (F_h), so that the user can feel a scaled version of the needle/tissue interaction forces.

Considering a steady-state (constant velocity) motion, it is possible to write the force balance equation (Figure 4.2) as:

$$F_h = F_a + F_f + F_t. \tag{4.3}$$

F_a in (4.2) can be replaced in (4.3), resulting in:

$$F_h(t) = -k_a(x_d(t) - x_a(t)) + F_f(t) + F_t(t). \tag{4.4}$$

The minus sign is added since F_a and x are defined as opposite in direction, as shown in Figure 4.2. Replacing x_d given in (4.1) and considering $F_e = F_t$, we obtain:

$$F_h = -k_a k_{if} \int_0^t (F_h - \alpha F_t)\, dt - k_a k_{pf}(F_h - \alpha F_t) + k_a x_a + F_f + F_t, \tag{4.5}$$

which can be rearranged as:

$$F_h + k_a k_{pf} F_h - \alpha\, k_a k_{pf} F_t - F_t = -k_a k_{if} \int_0^t (F_h - \alpha F_t) + k_a x_a + F_f. \tag{4.6}$$

Considering the simple case where the force feedback on the user hand (F_h) is not amplified ($\alpha = 1$), it is possible to compute the analytical solution. In a motion with constant velocity (v), $x_a(t) = v \cdot t$, F_f is proportional ($\mu =$ constant) to the depth of the needle inside the tissue

(x_a):

$$F_f(t) = \mu \cdot x_a(t) = \mu \cdot v \cdot t. \tag{4.7}$$

With $\alpha = 1$, we can rearrange (4.5) with respect to the force tracking error $e_f \quad (e_f = F_h - F_t)$:

$$(1 + k_a k_{pf})(F_h - F_t) = -k_a k_{if} \int_0^t (F_h - F_t) + k_a x_a + F_f, \tag{4.8}$$

and we obtain

$$(1 + k_a k_{pf}) e_f = -k_a k_{if} \int_0^t e_f dt + k_a \cdot vt + \mu \cdot vt. \tag{4.9}$$

The Laplace transform of (4.9) is

$$(1 + k_a k_{pf}) e_f(s) = -k_a k_{if} \frac{1}{s} \cdot e_f(s) + k_a v \frac{1}{s^2} + \mu v \frac{1}{s^2}. \tag{4.10}$$

Equation (4.10) can be rearranged as

$$e_f(s) = \frac{v \cdot k_a}{(1 + k_a k_{pf}) s^2 + k_a k_{if} s} + \frac{v \cdot \mu}{(1 + k_a k_{pf}) s^2 + k_a k_{if} s}. \tag{4.11}$$

Computing the inverse transform of (4.11), we obtain:

$$e(t) = \frac{v(\mu + k_a)}{k_a k_{if}} \left[1 - e^{-\frac{k_a k_{if}}{k_a k_{pf} + 1} t} \right] \tag{4.12}$$

and

$$F_h = \frac{v(\mu + k_a)}{k_a k_{if}} \left[1 - e^{-\frac{k_a k_{if}}{k_a k_{pf} + 1} t} \right] + F_t. \tag{4.13}$$

Equation (4.13) shows that the user always feels the tip force plus the contribution of the friction force (which depends on the insertion velocity, v, and on the friction coefficient μ), reduced by a factor proportional to the admittance gain k_{if} and k_a in the control loop. This contribution asymptotically reaches the maximum value for $t \to \infty$, where

$$F_h = \frac{v(\mu + k_a)}{k_a k_{if}} + F_t. \tag{4.14}$$

Thus, even if the force feedback amplification gain is unity ($\alpha = 1$), the user is able to perceive only the tip force plus a scaled contribution of the friction force, for k_{if} and k_a greater than one. Also, considering the case where velocity is close to zero, the hand force F_h is approximately equal to the tip force, $F_h \approx F_t$. This enables an enhanced perception of the needle-tissue interaction force at the needle tip on the operator hand, substantially reducing the friction force contribution.

In the *tip-friction* force control, (4.5) can be written as:

$$F_h = -k_a k_{if} \int_0^t (F_h - \alpha F_e)\, dt - k_a k_{pf}(F_h - \alpha F_e) + k_a x_a + F_e. \tag{4.15}$$

Thus, for $\alpha = 1$:

$$(1 + k_a k_{pf})(F_h - F_e) = -k_a k_{if} \int_0^t (F_h - F_e) + k_a x_a \tag{4.16}$$

and

$$(1 + k_a k_{pf}) e_f = -k_a k_{if} \int_0^t e_f dt + k_a x_a. \tag{4.17}$$

Applying the Laplace transform, we obtain:

$$(1 + k_a k_{pf}) e_f(s) = -k_a k_{if} \frac{1}{s} \cdot e_f(s) + k_a x_a(s) \tag{4.18}$$

and

$$e_f(s) = \frac{k_a s \cdot x_a(s)}{(1 + k_a k_{pf})s + k_a k_{if}}. \tag{4.19}$$

When x_a is a *step*, and we take the inverse transform,

$$F_h = \frac{k_a}{k_a k_{pf} + 1} \cdot e^{-\frac{k_a k_{if}}{k_a k_{pf}+1} t} + F_e. \tag{4.20}$$

The operator hand force is exactly equal to the environment force for $t \to \infty$ ($F_h = F_e$). When

x_a is a *ramp,* $x_a(\mathrm{t}) = v \cdot t$:

$$F_h = \frac{v}{k_{if}} \left[1 - e^{-\frac{k_a k_{if}}{k_a k_{pf}+1} t} \right] + F_e. \tag{4.21}$$

Here, for $t \to \infty$, F_h is equal to F_e plus a force contribution that depends on the slope (v) of the position *ramp* and which is scaled by k_{if}.

4.4 Comanipulation model simulation

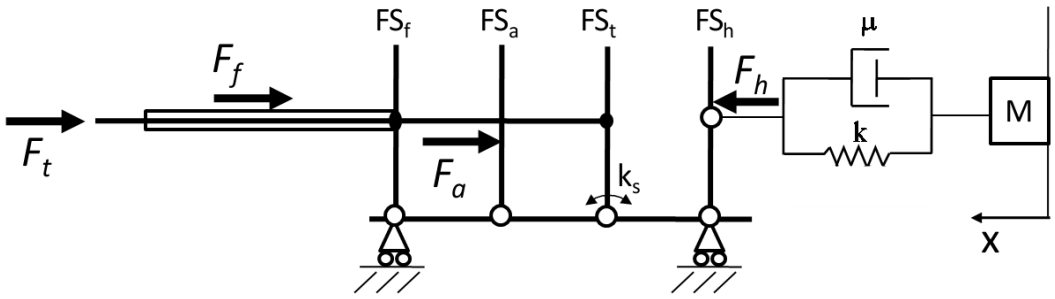

Figure 4.4: *Hand and device model simulated in the Simscape (Simulink 2011a, Mathworks) environment. F_h is the force exerted by the operator hand, F_t is the force acting only on the tip of the needle, F_f is the friction force between the needle and the surrounding tissue, F_a is the actuator force, and x is the positive direction of motion. FS_f, FS_a, FS_t and FS_h are the friction force sensor, actuator force sensor, tip force sensor and operator hand force sensor models, respectively. k_s is the elastic constant of the joint spring (sensor elasticity) linking each sensors to the sliding guide. k, μ and M are the elastic constant, the damping coefficient and the mass of the hand model, respectively [86].*

In order to analyze the system force tracking performance as a function of the variation of the force feedback amplification gain, α, we simulated the robotic coaxial needle insertion assistant system (Figure 4.4) using Simscape (Simulink 2011a, Mathworks).

Each force sensor (FS) was modelled as a beam with one angular degree of freedom. The beam is attached to a carriage with a spring, which models the elasticity of the beam itself. The applied tip force (F_t, Figure 4.5) was set to an initial constant force [0-15 seconds], then to an increasing ramp [15-27 seconds] with a quick drop to zero (which simulates the membrane rupture). The friction force (F_f) was modelled as a force constantly increasing with time (Figure 4.5). The desired hand position was given as an input to the model and was assumed to proceed with constant velocity. The actuator force (F_a) is then the output of the control loop, as shown

in Fig. 3. The hand was assumed to be a mass-spring-damper model with parameters derived from [50].

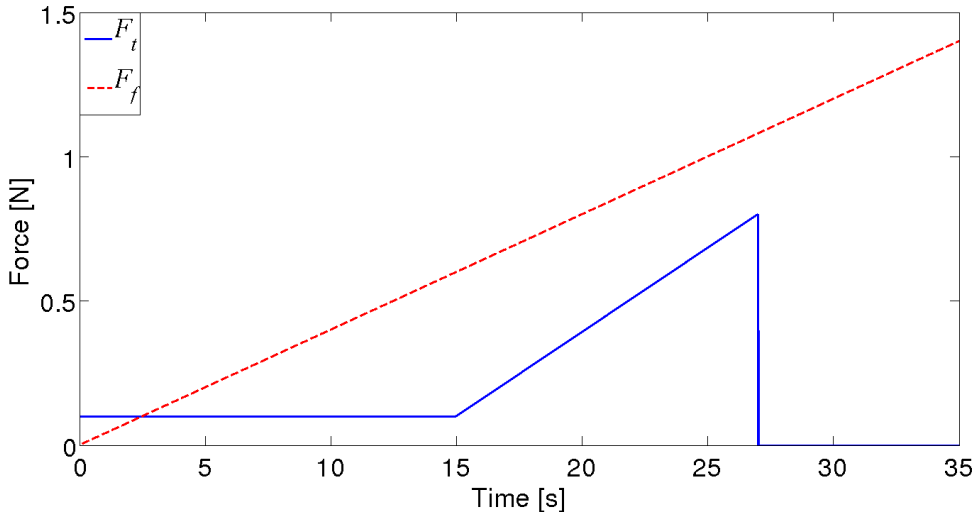

Figure 4.5: *Simulated friction force (F_f) and tip force (F_t) applied on the inner needle and on the outer needle respectively.*

In the simulations, the force feedback amplification gain (α) was varied from 1 to 40 and the admittance gains (k_{if} and k_{ip}) were empirically set equal to 200 mm/N and 300 mm/N·s, as a trade off between force tracking performance and stability of the control.

4.5 Experimental design and setup

4.5.1 Brain tissue mimicking material

In order to test the system performance in detecting brain vessels, six samples of Polyvinyl Chloride (PVC) rubber mimicking brain soft tissue were prepared. Two membranes made of silicone material (Smooth-on, 910) with 0.4 and 0.8 mm thicknesses, roughly resembling brain vessel walls, were placed inside the artificial soft tissue at three different depths: 15, 35, and 55 mm. The samples were prepared keeping the same compliance ratio between the brain parenchyma and the vessel walls. For brain parenchyma we used data from [86], while for the vessel walls we considered the work of Monson et al. [66]. The resulting ratio between brain and vessel compliance was 0.006.

4.5.2 Experimental protocol

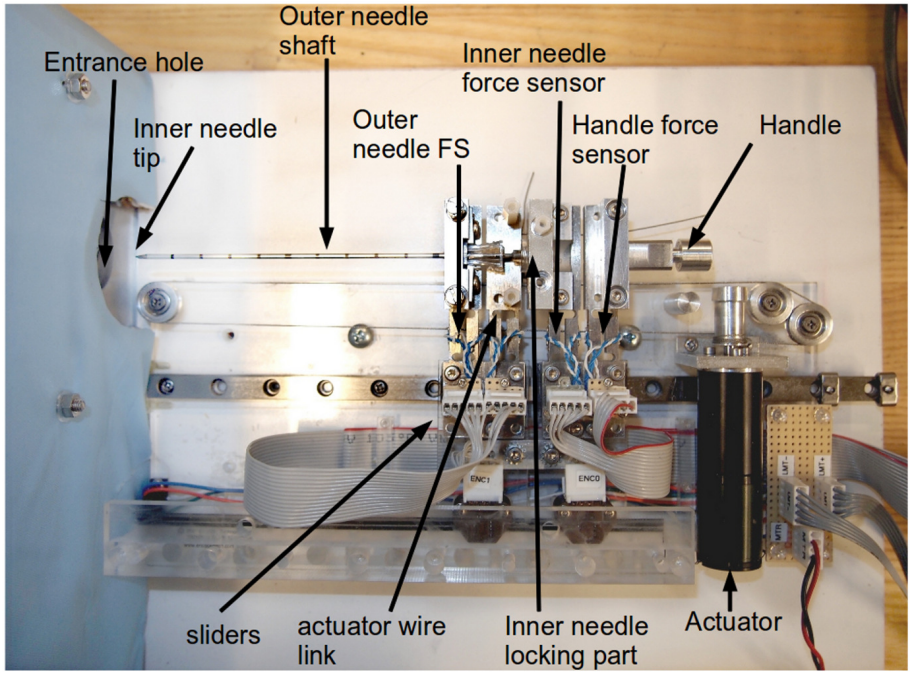

Figure 4.6: *Coaxial needle testing experimental setup. The blue sheet on the left is covering the tissue sample leaving only the entry point visible to the user*

A steel coaxial needle designed for biopsy with 2 mm diameter was used.

Eleven right-handed, neurologically healthy users participated in this study. The study was approved by the Johns Hopkins University Homewood Institutional Review Board. The users were seated, holding the handle of the needle with the right hand. The tissue was covered except for the entry point of the needles, so that the users could not visually discern the position of the membrane inside the samples (Figure 4.6). In each trial, one of two force feedback conditions were randomly displayed to the user:

- the tip force (*tip* force feedback),
- tip and friction force (*tip-friction* force feedback),

with the following pseudo-randomly varying conditions:

- two membrane thicknesses (0.4mm and 0.8mm),
- three membrane depths (15, 35, and 55 mm) and

- three different amplifications of feedback ($\alpha = 3, 6, 9$).

The insertion order for all these parameters was randomly changed among users. Each user performed 15 minutes of practice to understand the device behaviour. During the experiment, the number of insertions performed by each user was 36 and the total number of insertions performed by all users was 396.

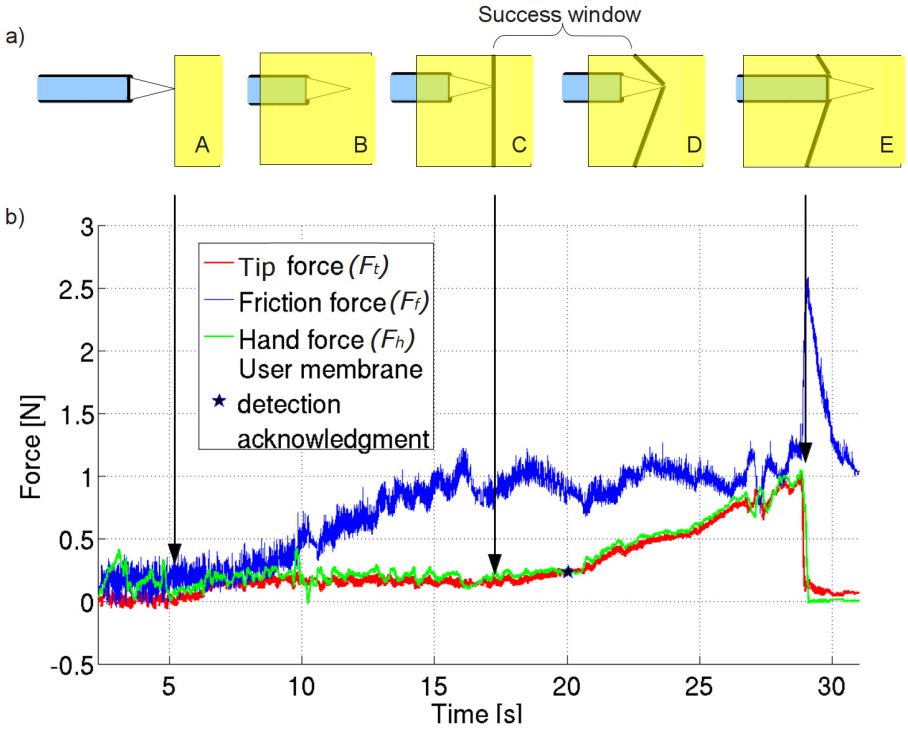

Figure 4.7: *(a) The phases and events of the needle insertion: free motion in air (A), surrounding tissue entering (B), membrane touching (C-D) and puncture (E). During user exeriments, subjects were asked to press a button as soon as they perceived contact with a membrane (between C and D), and stop moving the needle as soon as they detected that puncture had occurred (E). (b) Example of signals for a successful insertion with tip force feedback: the user detects the presence of the membrane before the puncture (star).*

Users were asked to blindly insert the biopsy needle into the sample and to press a button as soon as they perceived a membrane (Figure 4.7(a)). The time at which the button was pressed was recorded together with tip position and force data. The users were then asked to continue inserting the needle until they perceived a membrane puncture, and to stop advancing the needle immediately after the puncture occurred. The insertion was considered "successful" only if the user pressed the button within a time window that starts at the time the needle touches the membrane and ends immediately before the puncture occurs (Figure 4.7(a), between C and D).

The insertion was considered "unsuccessful" if the user pressed the button before the needle touched the membrane or after having punctured it or if the button was not pressed.

The success rate (number of successful events divided by the total number of trials) of membrane detection prior to puncturing using the two types of force display (*tip* force feedback and the *tip-friction* force feedback) was compared with a Wilcoxon test ($p<0.05$). The performance of the two force feedback conditions were compared combining different thicknesses and force amplification gains (α) (Wilcoxon and Chi-square tests, $p<0.05$).

Whenever the user pressed the button prior to reaching the membrane a "false positive detection" was considered to occur. The false positive ratio with respect to the membrane depth using the two force feedback conditions was compared (Wilcoxon test, $p<0.05$).

Whenever the user pressed the button after the puncturing of the membrane an "overshoot" was considered to occur. The overshoot ratio with respect to the membrane depth using the two force feedback conditions was compared (Wilcoxon test, $p<0.05$).

Also, the time to reach the membrane was computed as the temporal distance between the point where the needle start to touch the tissue sample and the point where it start to touch the membrane. This can also be considered as an average velocity prior to reach the membrane. The time to reach the membrane was compared using the two force feedback conditions, with respect to the depth of the membrane with a Wilcoxon test ($p<0.05$).

4.6 Results

4.6.1 Simulation results

Simulation results showed that the operator hand force (F_h) follows the shape of the tip force (F_t) (Figure 4.8). Increasing the force feedback amplification gain (α) results in reducing the force tracking error ($e_f = F_h - \alpha F_t$) (Figure 4.9) and the small oscillations visible in the top left panel of Figure 4.9 ($\alpha = 1$), for values of α less than 6. Figure 4.10 shows the Root Mean Square Errors (RMSE) between the scaled F_h and F_t with $\alpha = 1...40$. The RMSE on force tracking initially decreases with α increasing but then starts to grow again after $\alpha = 6$. Starting from $\alpha = 29$ the RMSE rapidly increases and the system becomes unstable.

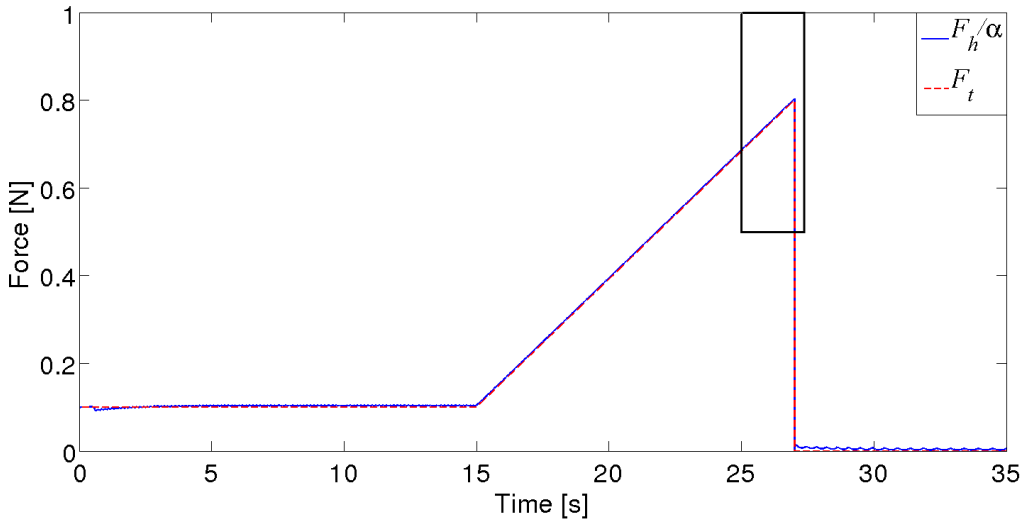

Figure 4.8: *Simulation results for $\alpha = 9$. Operator hand force (thick line) is already scaled by α in order to be superimposed to the tip force (F_t, dashed line). The black box is the signal window shown in Figure 4.9*

4.6.2 Experimental results

Figure 4.7(b) shows the tip force (F_t), friction force (F_f) and hand force (F_h) profiles, divided by the force gain (α). The tip force is almost constant when the needle is advancing in the artificial tissue (from 7 to 17 s), then F_t increases when the needle touches the membrane (at 17s). Then, the tip force drops rapidly after the membrane puncturing occurs (at 28 s). The friction force (F_f) gradually increases until the tip of the needle reaches the membrane (C). After that point, the tip force rapidly increases and the user perceives the force rapidly growing, while the friction force is almost constant. Immediately after the membrane puncture, the friction force rapidly increases because the membrane meets the outer needle and starts pushing it. After the user stops, the hand (F_h) and cutting force (F_t) go to zero, while F_f decreases to the value prior to the membrane touch. Figure 4.11 summarizes the performance of users with the two force feedback conditions in terms of success rate of membrane detection with respect to membrane depth. The success rate is always greater when only the *tip* force is displayed to the user (median 83% vs. 66% in case of a 15 mm membrane depth, 83% vs. 50% for 35 mm depth, and 50% vs. 0% for 55 mm depth). For the *tip-friction* force feedback, performance decreases with the depth of the membrane. Figure 4.12 shows detailed data for success rate in membrane detection with respect to both membrane depth and the various amplification gains.

Figure 4.9: *Simulation results with varying $\alpha = 1 \ldots 40$ from left to right and from top to bottom. The operator hand force, F_h (thick line), is scaled again by α in order to be superimposed to the tip force (F_t, dashed line). These graphs are the zoomed view of Figure 4.8 in the interval time [25 - 27.5 s].*

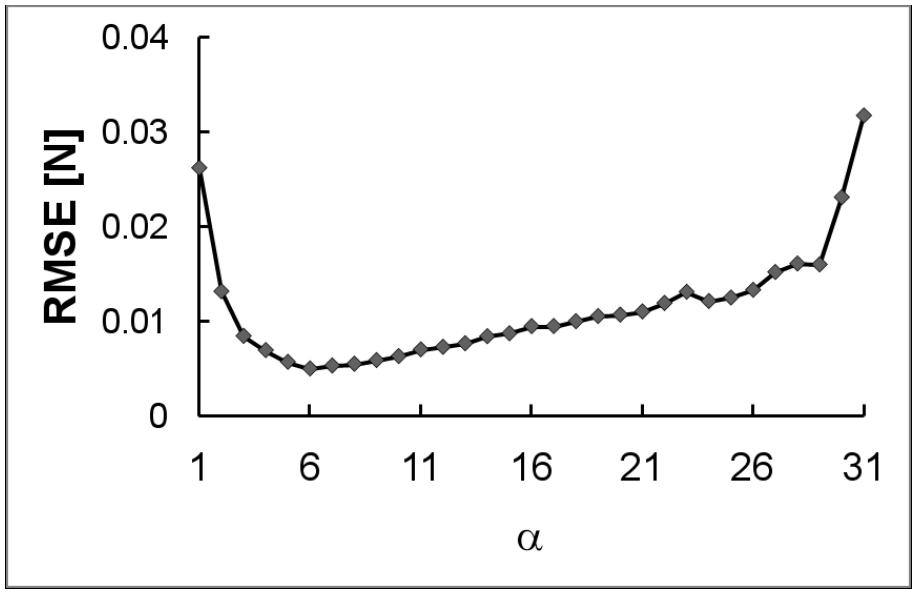

Figure 4.10: *Root mean squared error between F_h and F_t with α (tip force scaling gain) increasing from 1 to 31, based on a simulation with tip force feedback modality. The simulated signals used as force inputs are shown in Fig. 5 and the corresponding simulation results are shown in Figure 4.8 and Figure 4.9. See the text for explanation on the simulation environment.*

The performance of *tip* force feedback are significantly better than *tip-friction* force feedback (Chi-square $p < 0.03$) for high gains, but not for lower gains.

Table 4.2 shows the false positive ratio with respect to the membrane depth for both the force feedback type (*tip* and *tip-friction*). In case of *tip* force feedback, the false positive ratio is 0%, as a median value for deep membranes, while in case of *tip-friction* feedback the ratio reaches 83% as median value for the deepest membrane.

Table 4.2: *False Positives [%] for median and 5^{th} AND 95^{th} percentiles*

	15 [mm]			35 [mm]			55 [mm]		
	Median	5^{th}	95^{th}	Median	5^{th}	95^{th}	Median	5^{th}	95^{th}
Tip	0	0	16	0	0	0	0	0	33
Tip-Friction	0	0	17	33	0	99	83	0	100

Table 4.3 shows the overshoot ratio with respect to the membrane depth for both the force feedback type. The number of overshoots is close to zero as a median value among all the considered conditions, but the *tip-friction* case, where the median value is 17% for the 15mm

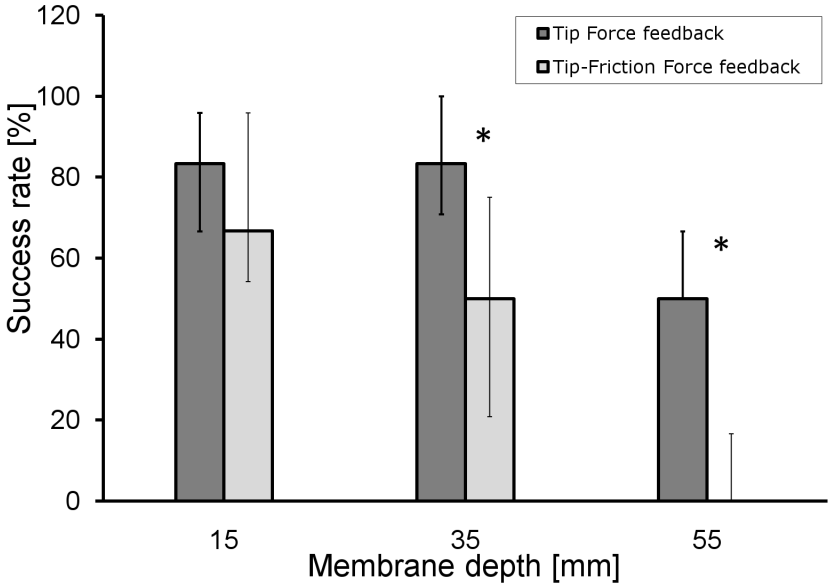

Figure 4.11: *Median success rate (see text for the explanation of the term) in membrane detection with respect to membrane depth and feedback type (tip force or tip-friction force feedback). The star indicates statistical significance, and the bars are the 25^{th} and 75^{th} percentile (note that for some histograms the percentile is coincident with the median).*

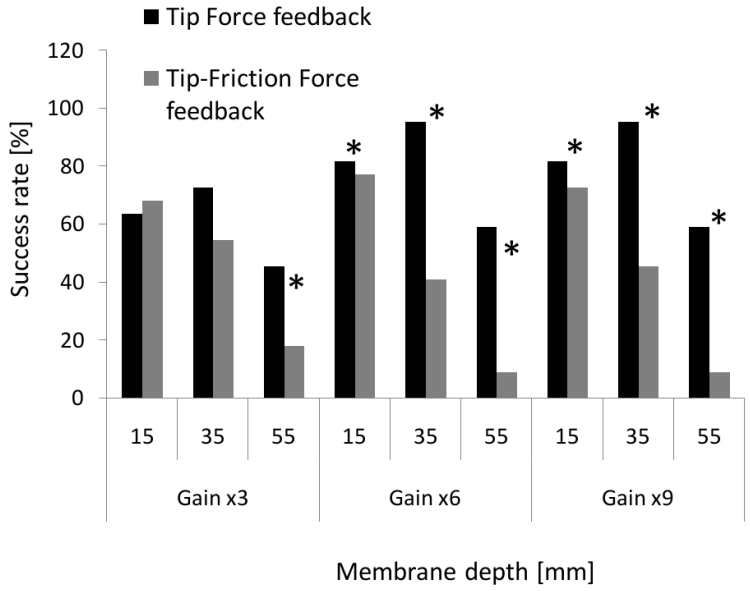

Figure 4.12: *Success rate in membrane detection with respect to membrane depth (15mm, 35mm and 35mm) and with different force amplification gains (α = 3, 6, 9) in the two force feedback cases (tip force or tip-friction force feedback). The star indicates statistical significance.*

membrane depth.

Table 4.3: *Overshoots [%] for median and 5^{th} AND 95^{th} percentiles*

	15 [mm]			35 [mm]			55 [mm]		
	Median	5^{th}	95^{th}	Median	5^{th}	95^{th}	Median	5^{th}	95^{th}
Tip	0	0	67	0	0	49	0	0	50
Tip-Friction	17	0	49	0	0	32	0	0	0

The median values of the time to reach the membrane (Figure 4.13) increases with the depth of the membrane as expected, but with a lower increment (i. e. higher insertion speed) for the *tip* force feedback. Also, the difference between the two force feedback type increases with the depth of membrane.

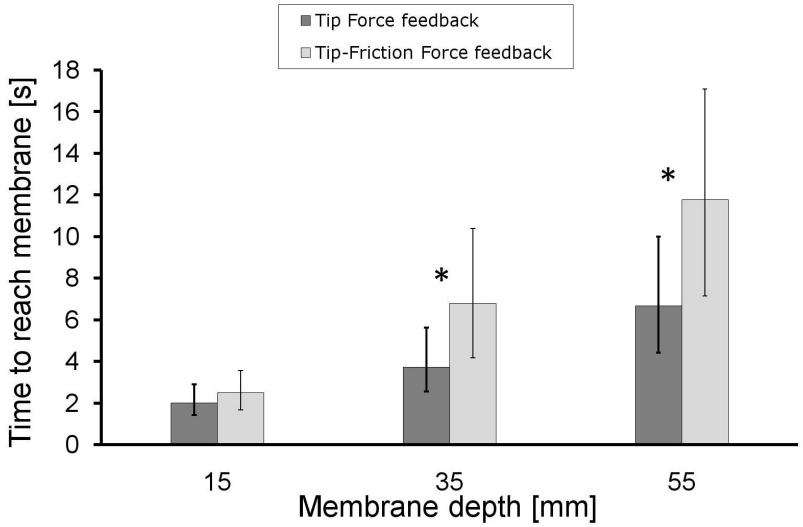

Figure 4.13: *Time to reach the membrane with respect the depth of the membrane for the two force feedback types. Median, 25th and 75th percentile. Wilcoxon test p-values (0.17, $2.02 \cdot 10^{-6}$, $5.95 \cdot 10^{-6}$)*

4.7 Discussion

In this chapter we showed a robotic coaxial needle assistant equipped with force sensors that allows a user to detect the interaction force between a needle tip and the surrounding soft tissue, thus enhancing the perception of tissue discontinuities during needle advancement. The paradigmatic application is keyhole neurosurgery, in which needles are inserted into the brain

parenchyma for biopsy, drug release or electrode placement. In such procedures, it is important to avoid damaging vessels along the needle path toward the target, particularly if lesions are located deep inside the brain. Bleeding inside the brain is the major source of complications in neurosurgery, so avoiding inadvertent puncture of vessels is important for patient safety [31]. With a conventional needle, soft membranes are generally not detectable because of the high noise due to the friction. In our approach, the user perceives only the contact force between the tip of the needle and the tissue, without feeling the increasing friction force along the shaft during the insertion, which complicates manual discrimination of changes in tissue properties. With respect to telemanipulation, the proposed cooperative manipulation control scheme allows the user to manipulate the same instrument that is performing the surgery and permits force-to-motion scaling [85].

In this work it was analytically and experimentally shown that the coaxial needle assistant facilitates the perception of thin membranes during the needle insertion when an amplified version of the tip force at the needle tip is displayed to the user. Even with coaxial needles, if the tip force is not amplified, membrane detection is difficult, due to the small amplitude of tip forces compared to total forces. Simulation results showed that increasing the force amplification gain allows better tip force trajectory tracking and reduces small oscillations due to the intrinsic sensors compliance (elasticity). Increasing the feedback amplification gain above $\alpha = 6$ does not improve the tracking error, but worsens it. The simulation does not consider the interaction force between the inner and the outer needle and the interfering forces acting perpendicular to the needle shaft. This can be further investigated, since in case of very thin needles, perpendicular forces can bend the needle and increase the friction force between the inner and the outer needle, thus lowering the quality of the force signal. Also, no soft tissue model was used, as we preferred to apply to the measured force profiles. A further analysis could consider including a viscoelastic soft tissue model [63].

Experimental results showed that the *tip* force feedback method performs better than displaying the overall interaction forces between the needle and the tissue (tip and friction forces together). This is an intuitive result, considering Weber's Law, which states that the ratio of the increment threshold to the background intensity is constant. In case of large background loads, small force variations are not felt by the human operator. As expected, the gap in performance

between the *tip* force feedback and the *tip-friction* force feedback increases with membrane depth inside the surrounding tissue; the larger the depth, the larger the friction force that masks the small force variations at the needle tip.

The force feedback gain significantly improves the performance of the *tip* force feedback with respect to the *tip-friction* force feedback, but for high force gain the overall performance is worsened. This could be due to increasing effort required by the operator to insert the needle, which degrades attention to force changes.

The *tip* force feedback significantly decreases false positive detection (close to zero). We desire the number of false positives to be as small as possible since false positives increase the procedure duration in clinical practice, due to repeated double-checking with other type of detection modalities (e.g. medical imaging).

Overshoots represent a small number of failures with respect to false positive detection for all the possible experimental conditions. In this specific task, users seems to behaved in a conservative approach, where the acknowledgement of a false positive detection is preferred to the overshoot and puncturing of the membrane.

The time to reach the membrane can be considered as the mean velocity that user used to insert the needle. With the *tip* force feedback we collected higher velocity of insertions with respect to the *tip-friction* approach. It seems that users moves more confidently and quickly with better feedback. No learnign curve was found during data analysis, so the average velocity of insertion was not increasing or decreasing with the insertion number for all the users.

The experiments were performed using samples of brain and vessel mimicking material. Artificial tissues are a necessity for repeatability of the stimulus between users. The difference in tissue compliance for the brain with respect to the vessels was derived from literature. Matching needle-tissue friction properties and fracture mechanics properties of the artificial tissues to real brain tissue would increase the relevance of our experiment, but such data for brain tissue are not available. However, the range of values for the interaction forces between the needle and the mimicking tissue (Figure 7(b)) are close to those found in literature for *ex vivo* needle insertion into swine brain parenchyma [29]. This latter are slightly lower than our data, but we can consider that they are an under estimation of the real forces expected in *in vivo* insertions, since the brain mechanical properties significantly and rapidly decreases with time, once

removed from the living being.

The remote configuration of the sensors, which are not positioned directly on the needle, allows detection of interaction forces using standard needles already used for biopsy. With this configuration, the needles are quickly and easily replaced and sterilization and miniaturization problems are solved. However, friction between the inner and outer needles degraded the haptic feedback to the user, especially for high force gain, since the user felt not only the cutting force at the tip of the needle, but also the friction force from the outer needle moving relative to the inner needle. In the experimental trials, attention to needle cleaning between each user experimental session solved the problem. Also, friction is correlated with misalignment between the outer needle and the inner one. Attention was paid in the apparatus design in order to ensure needle alignment.

Experiments showed that the choice of which force is displayed to the operator has a significant impact on performance. However, we did not consider the response time between the user perception of the membrane and the pressing of the button on the keyboard. Since this condition was the same in both the force feedback conditions, this did not affect our results. The ability of our system to display to the user only the tip force could help the operator in all the procedures that involve needle insertion, where the detection of membranes or different type of tissues can improve the performance or the success of the intervention.

The coaxial needle insertion assistant can be used also as a training tool for robotic surgery. Previous studies showed that the role of haptic feedback could be different for experienced and inexperienced surgeons [30] [67]. Our results are promising in terms of clinical practice, since we tested the device in a variety of different conditions that can be found in clinical practice and in all the conditions (membrane depths, membrane thicknesses, gain) enhanced perception performed well.

Together with cost and safety issues, one of challenges preventing the proliferation of robotic devices inside the operating room is the change of standard clinical protocol and instrumentation required in order to use the new technology. In this work, we showed that for needle insertion procedures it is possible to integrate force sensing with robotic devices, without changing the standard surgical needle, thus increasing safety and performance with relative low costs and inconvenience. The system will be carefully tested in preclinical conditions, such

as *ex vivo* biological tissues, to evaluate the clinical relevance.

CHAPTER 5

Conclusions

Force feedback in needle insertion robotic procedures has been widely investigated for surgical simulator [25], but during real scenario the literature is less widespread with respect to other typical surgical task like grasping or poking for laparoscopy. This work focused on the analysis of force sensing and display related issues for robotic needle insertion procedures. Two methodologies were analyzed for force detection and for enhancing force display through both a telerobotic surgical device and a comanipulated one.

For tasks such as tumour detection or the detection of arteries hidden underneath the tissue, force perception serves as determinative information for the medical decision. SurgeonâĂŹs ability to correctly judge in these situations is found to be based on the human compliance perception and compliance discrimination characteristics. Restoring the surgeonâĂŹs ability to differentiate between soft environments based on their stiffness/compliance therefore is crucial for needle insertions. Based on this insight, and the knowledge that human compliance percep-

tion is limited by both absolute and differential thresholds, we can distinguish three goals that we addressed in our work:

- Tissue compliance transparency need to be achieved in terms of offering a realistic feel of the tissue to discriminate between tissues as reliably as in open surgery. This means that direct measurements of the interaction forces between the environment and the surgical tool are indispensable to provide high quality touch feedback in a teleoperation or comanipulation setup. In Chapter 3 we investigated two force sensing modalities in order to validate the force accuracy detection with a force sensor and with a sensor-free approach in a specific neurosurgical scenario. For the latter, we were able to achieve force accuracy detection close to the force sensor approach and the quality of the sensing was assured by the absolute high accuracy (0.16N as maximum error) which is below the human JND and which should guarantee a satisfactory feedback. In the telemanipulation approach we did not analyzed the quality of force feedback with human subject experiment but we investigate it in Chapter 4, where the force sensing modality was even improved since we were able to sense different type of forces acting on the needle during the advancement, the force along the shaft and the force at the tip of the needle. Human subject experiments showed that the quality of force feedback was enough to discriminate between surrounding tissue and membrane. In both the approaches (telemanipulation and comanipulation) we avoided to place sensors directly on the needle, generally this introduces noise in the force signals, but has the advantage to eliminate sterilization and strong miniaturization issues. In our case, the noise in the force signals was below the JND.

  The main clinical application in our scenario was neurosurgery for the brain. In these procedures, the needle-tissue interaction force value range is below 1N and asks for customized sensors to be designed. We implemented customized sensors using strain gauge technology, which is reliable in terms of temperature drift correction in a bridge configuration with respect to other modalities such as optical sensors. We achieved 8.4mN resolution in the first approach and 4.2mN in the comanipulated device, which are values more than two orders of magnitude below the considered force range (0-1N),

- Some specific applications can benefit from scaled compliance transmission. Varying

force feedback gain allows to surmount absolute thresholds of human haptic perception. This can help for instance in brain or eye surgery, where forces often are too low to be perceived.

In Chapter 3 we did not analyzed the role of the amplification gain but we simulated and evaluated it in Chapter 4. In neurosurgical interventions the small force values ask for a scaled force feedback on the user hand in order to give the possibility to the surgeon to feel the needle-tissue interaction forces. The possibility to scale the feedback allows the user to feel forces otherwise not detectable. Although, we showed that the amplification gain plays a role in the stability of the system. In our case, a gain greater than 30 made the system to go unstable in the simulation results. In the real scenario, instability can be reached also for smaller gain values, since the simulation did not considered the position and force signal noises.

In the experimental trials we achieved a gain factor equal to 9 without any stability issues, which is enough to well amplify the needle tissue interaction forces for neurosurgical application. This could not be sufficient in other type of applications, like the eye surgery, where the interaction forces are even ten times smaller.

- A robotic system designed to enhance sensitivity, enables the surgeon to feel better than by bare hand and observe tinier stiffness differences. Thus, human differential haptic thresholds are overcome. From a clinical point of view, this technique is expected to raise the confidence level for the detection of soft tissue mechanical property changes, or to increase the accuracy in blind needle positioning. Simulations and experiments showed we were able to enhance the human ability to detect small amount of forces and small tissue compliance differences, by the separation of the force contributions acting on the needle during insertion into soft tissues. This was achieved using dedicated force sensors placed far from the needle tip and an admittance control algorithm which was able to enhance only the needle tip - tissue force exchange to be presented to the user. This approach showed a great potential in incrementing detection of membrane accuracy, thus lowering the potential risks associated with unwanted membrane puncturing. The experimental results showed that even the false positive membrane detection decreases, given

a possibility to improve the performances in specific applications where the knowledge of the presence of a membrane is important for the final outcome of the procedure (for instance, in epidural anesthesia, the knowledge of having punctured the membrane and reached the epidural space is important for the final efficacy of the drug delivery and to prevent annoying side effects, like headache).

We achieved the mentioned goals validating force sensing and force display capabilities in controlled environmental conditions close to neurosurgical interventions. The use of artificial material samples to mimic real tissues from one side allowed us to have reliable results with controlled experimental conditions, from another point of view this constraints our results in specific conditions which can be different from the real conditions in human soft tissues.

In the next future, pre-clinical and clinical evaluations should verify the expectations that enhanced force feedback in needle insertion tasks enables surgeons to localise, identify and determine the boundaries of tissue properties or arteries/veins with a higher confidence level and better accuracy.

Future works can extend the features of the devices in terms of on board "intelligence" that can help the surgeon in several situations. In particular, the high level control:

- can limit the needle advancement velocity depending on the anatomical or functional area of the body to be traversed
- can alert the surgeon before the needle puncture an important structure or membrane and stop at a specific location.
- can on-line correct the needle position in case of change of target position due to soft tissue motion (e.g. going slightly back after puncture of membrane and overshooting during an epidural anaesthesia task).

In our work, we did not take into considerations all the forces acting perpendicular to the direction of the needle motion. So far, we considered these forces neglectable, further studies can improve the force detection also in other directions. Future work can investigate the use of vibratory motion actuated by piezoelements in order to determine if this can reduce the needle-tissue interaction forces and, consequently the tissue stress and/or damage.

Also, methods for online mechanical property of the tissue could be studied using vibratory actuation in order to predict a change of type of tissue during the needle path (for instance, to detect the presence of a tumor or a cyst).

We showed that for needle insertion procedures it is possible to integrate force sensing with robotic devices, without changing the standard surgical needle and surgical workflow modality, thus increasing safety and performances with relative low costs.

List of Figures

List of Tables

Bibliography

[1] J. J. Abbott and A. M. Okamura. Virtual fixture architectures for telemanipulation. In *Robotics and Automation, 2003. Proceedings. ICRA '03. IEEE International Conference on*, volume 2, pages 2798–2805 vol.2, 2003.

[2] N. Abolhassani, R. Patel, and M. Moallem. Trajectory generation for robotic needle insertion in soft tissue. *Annual International Conference of the IEEE Engineering in Medicine and Biology Society.IEEE Engineering in Medicine and Biology Society.Conference*, 4:2730–2733, 2004.

[3] Niki Abolhassani, Rajni Patel, and Mehrdad Moallem. Needle insertion into soft tissue: A survey. *Medical engineering & physics*, 29(4):413–431, 5 2007.

[4] Ali Asadian, Rajni V. Patel, and Mehrdad R. Kermani. A distributed model for needle-tissue friction in percutaneous interventions. In *Robotics and Automation (ICRA), 2011 IEEE International Conference on*, pages 1896–1901, 2011.

[5] F. S. Azar, D. N. Metaxas, and M. D. Schnall. A finite element model of the breast for predicting mechanical deformations during biopsy procedures. In *Mathematical Methods in Biomedical Image Analysis, 2000. Proceedings. IEEE Workshop on*, pages 38–45, 2000.

[6] N. H. Bakker, P. J. Werkhoven, and P. O. Passenier. Aiding orientation performance in virtual environments with proprioceptive feedback. In *Virtual Reality Annual International Symposium, 1998. Proceedings., IEEE 1998*, pages 28–33, 1998.

[7] L. Barbe, B. Bayle, M. de Mathelin, and A. Gangi. In vivo model estimation and haptic characterization of needle insertions. *The International Journal of Robotics Research*, 26(11-12):1283–1301, November 01 2007.

[8] L. Barbé, B. Bayle, M. de Mathelin, and A. Gangi. Needle insertions modeling: Identifiability and limitations. *Biomedical Signal Processing and Control*, 2(3):191–198, 7 2007.

[9] C. W. Berger, E. T. Crosby, and W. Grodecki. North american survey of the management of dural puncture occurring during labour epidural analgesia. *Canadian journal of anaesthesia*, 45(2):110–114, Feb 1998.

[10] B. T. Bethea, A. M. Okamura, M. Kitagawa, T. P. Fitton, S. M. Cattaneo, V. L. Gott, W. A. Baumgartner, and D. D. Yuh. Application of haptic feedback to robotic surgery. *Journal of laparoendoscopic & advanced surgical techniques.Part A*, 14(3):191–195, Jun 2004.

[11] A. Bicchi, G. Canepa, D. De Rossi, P. Iacconi, and E. P. Scillingo. A sensor-based minimally invasive surgery tool for detecting tissue elastic properties. In *1996 IEEE International Conference on Robotics and Automation*, volume 1, pages 884–888 vol.1, 1996.

[12] D. H. Boehm, H. Reichenspurner, C. Detter, M. Arnold, H. Gulbins, B. Meiser, and B. Reichart. Clinical use of a computer-enhanced surgical robotic system for endoscopic coronary artery bypass grafting on the beating heart. *The Thoracic and cardiovascular surgeon*, 48(4):198–202, Aug 2000.

[13] J. D. Brown, J. Rosen, M. Moreyra, M. Sinanan, and B. Hannaford. Computer-controlled motorized endoscopic grasper for in vivo measurement of soft tissue biomechanical characteristics. *Studies in health technology and informatics*, 85:71–73, 2002.

[14] C. G. L. Cao, M. Zhou, D. B. Jones, and S. D. Schwaitzberg. Can surgeons think and operate with haptics at the same time? *Journal of Gastrointestinal Surgery*, 11(11):1564–1569, 2007.

[15] A. Carra and J. C. Avila-Vilchis. Needle insertion modeling through several tissue layers. In *Informatics in Control, Automation and Robotics (CAR), 2010 2nd International Asia Conference on*, volume 1, pages 237–240, 2010.

[16] K. Cleary, M. Freedman, M. Clifford, D. Lindisch, S. Onda, and L. Jiang. Image-guided robotic delivery system for precise placement of therapeutic agents. *Journal of Controlled Release*, 74(1-3):363–368, 7/6 2001.

[17] M. Cossu, G. Lo Russo, S. Francione, R. Mai, L. Nobili, I. Sartori, L. Tassi, A. Citterio, N. Colombo, M. Bramerio, C. Galli, L. Castana, and F. Cardinale. Epilepsy surgery in children: results and predictors of outcome on seizures. *Epilepsia*, 49(1):65–72, Jan 2008.

[18] Jessica Crouch, Chad Schneider, Josh Wainer, and Allison Okamura. *A Velocity-Dependent Model for Needle Insertion in Soft Tissue*, volume 3750 of *Medical Image Computing and Computer-Assisted Intervention - MICCAI 2005*, pages 624–632. Springer Berlin / Heidelberg, 2005.

[19] P. Dario, B. Hannaford, and A. Menciassi. Smart surgical tools and augmenting devices. *Robotics and Automation, IEEE Transactions on*, 19(5):782–792, 2003.

[20] Prokar Dasgupta, Adam Jones, and Inderbir S. Gill. Robotic urological surgery: a perspective. *BJU international*, 95(1):20–23, 2005.

[21] B. Davies, M. Jakopec, S. J. Harris, F. Rodriguez y Baena, A. Barrett, A. Evangelidis, P. Gomes, J. Henckel, and J. Cobb. Active-constraint robotics for surgery. *Proceedings of the IEEE*, 94(9):1696–1704, 2006.

[22] G. Deacon, A. Harwood, J. Holdback, D. Maiwand, M. Pearce, I. Reid, M. Street, and J. Taylor. The pathfinder image-guided surgical robot. *Proceedings of the Institution of Mechanical Engineers.Part H, Journal of engineering in medicine*, 224(5):691–713, 2010.

[23] B. Demi, T. Ortmaier, and U. Seibold. The touch and feel in minimally invasive surgery. In *Haptic Audio Visual Environments and their Applications, 2005. IEEE International Workshop on*, page 6 pp., 2005.

[24] der Putten Westebring van, R. H. M. Goossens, J. J. Jakimowicz, and J. Dankelman. Haptics in minimally invasive surgery - a review. *Minim Invasive Ther Allied Technol*, 17(1):3–16, 01/01; 2012/01 2008.

[25] S. P. DiMaio and S. E. Salcudean. Needle insertion modeling and simulation. *Robotics and Automation, IEEE Transactions on*, 19(5):864–875, 2003.

[26] L. H. Eadie, A. M. Seifalian, and B. R. Davidson. Telemedicine in surgery. *British Journal of Surgery*, 90(6):647–658, 2003.

[27] M. S. Eljamel. Validation of the pathfinder neurosurgical robot using a phantom. *The International Journal of Medical Robotics and Computer Assisted Surgery*, 3(4):372–377, 2007.

[28] J. A. Engh, G. Podnar, S. Y. Khoo, and C. N. Riviere. Flexible needle steering system for percutaneous access to deep zones of the brain. In *Bioengineering Conference, 2006. Proceedings of the IEEE 32nd Annual Northeast*, pages 103–104, 2006.

[29] L. Frasson, T. Parittotokkaporn, A. Schneider, B. L. Davies, J. F. V. Vincent, S. E. Huq, P. Degenaar, and F. M. Rodriguez Baena. Biologically inspired microtexturing: Investigation into the surface topography of next-generation neurosurgical probes. In *Engineering in Medicine and Biology Society, 2008. EMBS 2008. 30th Annual International Conference of the IEEE*, pages 5611–5614, 2008.

[30] Oleg Gerovich, Panadda Marayong, and Allison M. Okamura. The effect of visual and haptic feedback on computer-assisted needle insertion*. *Computer Aided Surgery*, 9(6):243–249, 01/01; 2011/11 2004.

[31] R. Grossman, S. Sadetzki, R. Spiegelmann, and Z. Ram. Haemorrhagic complications and the incidence of asymptomatic bleeding associated with stereotactic brain biopsies. *Acta Neurochirurgica*, 147(6):627–631, 2005.

[32] James C. Gwilliam, Mohsen Mahvash, Balazs Vagvolgyi, Alexander Vacharat, David D. Yuh, and Allison M. Okamura. Effects of haptic and graphical force feedback on teleoperated palpation. In *Robotics and Automation, 2009. ICRA '09. IEEE International Conference on*, pages 677–682, 2009.

[33] P. J. Hacksel and S. E. Salcudean. Estimation of environment forces and rigid-body velocities using observers. In *Robotics and Automation, 1994. Proceedings., 1994 IEEE International Conference on*, pages 931–936 vol.2, 1994.

[34] G. Hager, A. Okamura, P. Kazanzides, L. Whitcomb, G. Fichtinger, and R. Taylor. Surgical and interventional robotics: part iii [tutorial]. *Robotics & Automation Magazine, IEEE*, 15(4):84–93, 2008.

[35] Ulrich Hagn, R. Konietschke, A. Tobergte, M. Nickl, S. Jörg, B. Kübler, G. Passig, M. Gröger, F. Fröhlich, U. Seibold, L. Le-Tien, A. Albu-Schäffer, A. Nothhelfer, F. Hacker, M. Grebenstein, and G. Hirzinger. Dlr mirosurge: a versatile system for research in endoscopic telesurgery. *International Journal of Computer Assisted Radiology and Surgery*, 5(2):183–193, 2010.

[36] B. Hannaford. A design framework for teleoperators with kinesthetic feedback. *Robotics and Automation, IEEE Transactions on*, 5(4):426–434, 1989.

[37] Keyvan Hashtrudi-Zaad and Septimiu E. Salcudean. Analysis of control architectures for teleoperation systems with impedance/admittance master and slave manipulators. *The International Journal of Robotics Research*, 20(6):419–445, June 01 2001.

[38] E. A. Heijnsdijk, A. Pasdeloup, A. J. van der Pijl, J. Dankelman, and D. J. Gouma. The influence of force feedback and visual feedback in grasping tissue laparoscopically. *Surgical endoscopy*, 18(6):980–985, Jun 2004.

[39] M. N. Helmus, D. F. Gibbons, and D. Cebon. Biocompatibility: meeting a key functional requirement of next-generation medical devices. *Toxicologic pathology*, 36(1):70–80, Jan 2008.

[40] M. N. Hochman and M. J. Friedman. An in vitro study of needle force penetration comparing a standard linear insertion to the new bidirectional rotation insertion technique. *Quintessence international (Berlin, Germany : 1985)*, 32(10):789–796, Nov-Dec 2001.

[41] H. K. Hussain, J. E. Kingston, P. Domizio, A. J. Norton, and R. H. Reznek. Imaging-guided core biopsy for the diagnosis of malignant tumors in pediatric patients. *AJR.American journal of roentgenology*, 176(1):43–47, Jan 2001.

[42] M. A. Howard III, B. A. Abkes, M. C. Ollendieck, M. D. Noh, C. Ritter, and G. T. Gillies. Measurement of the force required to move a neurosurgical probe through in vivo human brain tissue. *Biomedical Engineering, IEEE Transactions on*, 46(7):891–894, 1999.

[43] L. A. Jones. Matching forces: constant errors and differential thresholds. *Perception*, 18(5):681–687, 1989.

[44] Werner A. Kaiser, Harald Fischer, Jeorg Vagner, and Manfred Selig. Robotic system for biopsy and therapy of breast lesions in a high-field whole-body magnetic resonance tomography unit. *Investigative radiology*, 35(8), 2000.

[45] S. Katsura, Y. Matsumoto, and K. Ohnishi. Analysis and experimental validation of force bandwidth, for force control rid f-4513-2010 rid a-6543-2011. *IEEE Transactions on Industrial Electronics*, 53(3):922–928, JUN 2006.

[46] Ryo Kikuuwe, Yu Kobayashi, and Hideo Fujimoto. Coulomb-friction-based needle insertion/withdrawal model and its discrete-time implementation. In *EuroHaptics 2006*, pages 207–212, jul 2006.

[47] M. Kitagawa, D. Dokko, A. M. Okamura, and D. D. Yuh. Effect of sensory substitution on suture-manipulation forces for robotic surgical systems. *The Journal of thoracic and cardiovascular surgery*, 129(1):151–158, Jan 2005.

[48] M. Kitagawa, D. Dokko, A. M. Okamura, and D. D. Yuh. Effect of sensory substitution on suture-manipulation forces for robotic surgical systems. *Journal of Thoracic and Cardiovascular Surgery*, 129(1):151–158, 2005.

[49] F. W. Kreth, A. Muacevic, R. Medele, K. Bise, T. Meyer, and H. J Reulen. The risk of haemorrhage after image guided stereotactic biopsy of intra-axial brain tumours - a prospective study. *Acta Neurochirurgica*, 143(6):539–546, 2001.

[50] Katherine J. Kuchenbecker, June Gyu Park, and Gunter Niemeyer. Characterizing the human wrist for improved haptic interaction. *ASME Conference Proceedings*, 2003(37130):591–598, January 1, 2003 2003.

[51] B. Kuebler, U. Seibold, and G. Hirzinger. Development of actuated and sensor integrated forceps for minimally invasive robotic surger. *The International Journal of Medical Robotics and Computer Assisted Surgery*, 1(3):96–107, 2005.

[52] Abhaya V. Kulkarni, Abhijit Guha, Andres Lozano, and Mark Bernstein. Incidence of silent hemorrhage and delayed deterioration after stereotactic brain biopsy. *Journal of neurosurgery*, 89(1):31–35, 07/01; 2011/11 1998.

[53] Dong-Soo Kwon, Ki Young Woo, Se Kyong Song, Wan Soo Kim, and Hyung Suck Cho. Microsurgical telerobot system. In *Proceeding of the 1998 IEEE/RS International Conference on Intelligent Robots and Systems*, volume 2, pages 945–950 vol.2, 1998.

[54] H. Y. K. Lau and L. C. C. Wai. Implementation of position-force and position-position teleoperator controllers with cable-driven mechanisms. *Robotics and Computer-Integrated Manufacturing*, 21(2):145–152, 4 2005.

[55] D. A. Lawrence. Stability and transparency in bilateral teleoperation. *Robotics and Automation, IEEE Transactions on*, 9(5):624–637, 1993.

[56] M. Lazeroms, G. Villavicencio, W. Jongkind, and G. Honderd. Optical fibre force sensor for minimal-invasive-surgery grasping instruments. In *Engineering in Medicine and Biology Society, 1996. Bridging Disciplines for Biomedicine. Proceedings of the 18th Annual International Conference of the IEEE*, volume 1, pages 234–235 vol.1, 1996.

[57] Sangyoon Lee and Gerard Jounghyun Kim. Effects of haptic feedback, stereoscopy, and image resolution on performance and presence in remote navigation. *International Journal of Human-Computer Studies*, 66(10):701–717, 10 2008.

[58] Mohsen Mahvash and Allison Okamura. Friction compensation for enhancing transparency of a teleoperator with compliant transmission rid a-3323-2010. *Ieee Transactions on Robotics*, 23(6):1240–1246, DEC 2007.

[59] H. R. Malone, O. N. Syed, M. S. Downes, A. L. D'Ambrosio, D. O. Quest, and M. G. Kaiser. Simulation in neurosurgery: a review of computer-based simulation environments and their surgical applications. *Neurosurgery*, 67(4):1105–1116, Oct 2010.

[60] G. L. McCreery, A. L. Trejos, M. D. Naish, R. V. Patel, and R. A. Malthaner. Feasibility of locating tumours in lung via kinaesthetic feedback. *The international journal of medical robotics & computer assisted surgery*, 4(1):58–68, Mar 2008.

[61] G. C. Mendes, T. R. Brandao, and C. L. Silva. Ethylene oxide sterilization of medical devices: a review. *American Journal of Infection Control*, 35(9):574–581, Nov 2007.

[62] Mani Menon, Ashok K. Hemal, Ashutosh Tewari, Alok Shrivastava, Ahmed M. Shoma, Hassan Abol-Ein, and Mohamed A. Ghoneim. Robot-assisted radical cystectomy and urinary diversion in female patients: technique with preservation of the uterus and vagina. *Journal of the American College of Surgeons*, 198(3):386–393, 3 2004.

[63] S. Misra, K. T. Ramesh, and A. M. Okamura. Modeling of tool-tissue interactions for computer-based surgical simulation: A literature review. *Presence (Cambridge, Mass.)*, 17(5):463, Oct 1 2008.

[64] F. W. Mohr, J. F. Onnasch, V. Falk, T. Walther, A. Diegeler, R. Krakor, F. Schneider, and R. Autschbach. The evolution of minimally invasive valve surgery–2 year experience. *European journal of cardio-thoracic surgery : official journal of the European Association for Cardio-thoracic Surgery*, 15(3):233–8; discussion 238–9, Mar 1999.

[65] E. De Momi and G. Ferrigno. Robotic and artificial intelligence for keyhole neurosurgery: the robocast project, a multi-modal autonomous path planner. *Proceedings of the Institution of Mechanical Engineers Part H-Journal of Engineering in Medicine*, 224(H5):715–727, 2010.

[66] Kenneth L. Monson, Werner Goldsmith, Nicholas M. Barbaro, and Geoffrey T. Manley. Significance of source and size in the mechanical response of human cerebral blood vessels. *Journal of Biomechanics*, 38(4):737–744, 4 2005.

[67] P. C. Mozer, A. W. Partin, and D. Stoianovici. Robotic image-guided needle interventions of the prostate. *Reviews in urology*, 11(1):7–15, Winter 2009.

[68] S. Nath, Z. Chen, N. Yue, S. Trumpore, and R. Peschel. Dosimetric effects of needle divergence in prostate seed implant using 125i and 103pd radioactive seeds. *Medical physics*, 27(5):1058–1066, May 2000.

[69] A. M. Okamura. Methods for haptic feedback in teleoperated robot-assisted surgery. *The Industrial robot*, 31(6):499–508, Dec 2004.

[70] A. M. Okamura. Haptic feedback in robot-assisted minimally invasive surgery. *Current opinion in urology*, 19(1):102–107, Jan 2009.

[71] A. M. Okamura, C. Simone, and M. D. O'Leary. Force modeling for needle insertion into soft tissue. *Biomedical Engineering, IEEE Transactions on*, 51(10):1707–1716, 2004.

[72] X. D. Pang, H. Z. Tan, and N. I. Durlach. Manual discrimination of force using active finger motion. *Perception & psychophysics*, 49(6):531–540, Jun 1991.

[73] Jan Peirs, Joeri Clijnen, Dominiek Reynaerts, Hendrik Van Brussel, Paul Herijgers, Brecht Corteville, and Sarah Boone. A micro optical force sensor for force feedback during minimally invasive robotic surgery. *Sensors and Actuators A: Physical*, 115(2-3):447–455, 9/21 2004.

[74] J. O. Perreault and C. G. Cao. Effects of vision and friction on haptic perception. *Human factors*, 48(3):574–586, Fall 2006.

[75] P. Puangmali, K. Althoefer, L. D. Seneviratne, D. Murphy, and P. Dasgupta. State-of-the-art in force and tactile sensing for minimally invasive surgery. *Sensors Journal, IEEE*, 8(4):371–381, 2008.

[76] C. E. Reiley, T. Akinbiyi, D. Burschka, D. C. Chang, A. M. Okamura, and D. D. Yuh. Effects of visual force feedback on robot-assisted surgical task performance. *The Journal of thoracic and cardiovascular surgery*, 135(1):196–202, Jan 2008.

[77] P. Richard and P. Coiffet. Human perceptual issues in virtual environments: sensory substitution and information redundancy. In *Proceedings of the 4th IEEE International Workshop on Robot and Human Communication*, pages 301–306, 1995.

[78] R. C. Ritter, E. G. Quate, G. T. Gillies, M. S. Grady, M. A. Howard III, and W. C. Broaddus. Measurement of friction on straight catheters in in vitro brain and phantom material. *Biomedical Engineering, IEEE Transactions on*, 45(4):476–485, 1998.

[79] Cameron N. Riviere, Jacques Gangloff, and Michel de Mathelin. Robotic compensation of biological motion to enhance surgical accuracy. *Proceedings of the IEEE*, 94(9):1705–1716, SEP 2006.

[80] P. R. Rizun, P. B. McBeth, D. F. Louw, and G. R. Sutherland. Robot-assisted neurosurgery. *Seminars in laparoscopic surgery*, 11(2):99–106, Jun 2004.

[81] P. L. Roberson, V. Narayana, D. L. McShan, R. J. Winfield, and P. W. McLaughlin. Source placement error for permanent implant of the prostate. *Medical physics*, 24(2):251–257, Feb 1997.

[82] J. Rosen, B. Hannaford, MP MacFarlane, and MN Sinanan. Force controlled and teleoperated endoscopic grasper for minimally invasive surgery - experimental performance evaluation. *IEEE Transactions on Biomedical Engineering*, 46(10):1212–1221, OCT 1999.

[83] A. Rossi, A. Trevisani, and V. Zanotto. A telerobotic haptic system for minimally invasive stereotactic neurosurgery. *The International Journal of Medical Robotics and Computer Assisted Surgery*, 1(2):64–75, 2005.

[84] J. Roy, D. L. Rothbaum, and L. L. Whitcomb. Haptic feedback augmentation through position based adaptive force scaling: theory and experiment. In *IEEE/RSJ International Conference on Intelligent Robots and Systems*, volume 3, pages 2911–2919 vol.3, 2002.

[85] J. Roy and L. L. Whitcomb. Adaptive force control of position/velocity controlled robots: theory and experiment. *IEEE Transactions on Robotics and Automation*, 18(2):121–137, 2002.

[86] I. Sack, B. Beierbach, J. Wuerfel, D. Klatt, U. Hamhaber, S. Papazoglou, P. Martus, and J. Braun. The impact of aging and gender on brain viscoelasticity. *NeuroImage*, 46(3):652–657, Jul 1 2009.

[87] S. E. Salcudean and J. Yan. Towards a force-reflecting motion-scale system for microsurgery. In *Proceedings of the IEEE International Conference on Robotics and Automation*, pages 2296–2301 vol.3, 1994.

[88] Oliver A. Shergold and Norman A. Fleck. Experimental investigation into the deep penetration of soft solids by sharp and blunt punches, with application to the piercing of skin. *Journal of Biomechanical Engineering*, 127(5):838–848, October 2005 2005.

[89] K. B. Shimoga. A survey of perceptual feedback issues in dexterous telemanipulation. ii. finger touch feedback. In *Virtual Reality Annual International Symposium, 1993., 1993 IEEE*, pages 271–279, 1993.

[90] M. Shoham, M. Burman, E. Zehavi, L. Joskowicz, E. Batkilin, and Y. Kunicher. Bone-mounted miniature robot for surgical procedures: Concept and clinical applications. *IEEE Transactions on Robotics and Automation*, 19(5):893–901, 2003.

[91] Hyoung Il Son, Tapomayukh Bhattacharjee, and Doo Yong Lee. Estimation of environmental force for the haptic interface of robotic surgery rid c-1534-2011. *International Journal of Medical Robotics and Computer Assisted Surgery*, 6(2):221–230, JUN 2010.

[92] J. E. Speich, K. Fite, and M. Goldfarb. A method for simultaneously increasing transparency and stability robustness in bilateral telemanipulation. In *Proceedings of the IEEE International Conference on Robotics and Automation, ICRA 2000*, volume 3, pages 2671–2676 vol.3, 2000.

[93] Garnette R. Sutherland, Isabelle Latour, and Alexander D. Greer. A general-purpose mr-compatible robotic system. *IEEE Engineering in Medicine and Biology Magazine*, 27(3):59–65, MAY-JUN 2008.

[94] Rupesh Tarwala and Lawrence Dorr. Robotic assisted total hip arthroplasty using the mako platform. *Current Reviews in Musculoskeletal Medicine*, 4(3):151–156, 2011.

[95] R. Taschereau, J. Pouliot, J. Roy, and D. Tremblay. Seed misplacement and stabilizing needles in transperineal permanent prostate implants. *Radiotherapy and oncology : journal of the European Society for Therapeutic Radiology and Oncology*, 55(1):59–63, Apr 2000.

[96] M. Tavakoli, R. V. Patel, and M. Moallem. Haptic feedback and sensory substitution during telemanipulated suturing. In *First Joint Eurohaptics Conference, 2005 and Symposium on Haptic Interfaces for Virtual Environment and Teleoperator Systems 2005*, pages 543–544, 2005.

[97] M. Tavakoli, R. V. Patel, and M. Moallem. Bilateral control of a teleoperator for soft tissue palpation: design and experiments. In *Proceedings of the IEEE International Conference on Robotics and Automation, ICRA 2006*, pages 3280–3285, 2006.

[98] G. Tholey, J. P. Desai, and A. E. Castellanos. Force feedback plays a significant role in minimally invasive surgery: Results and analysis. *Annals of Surgery*, 241(1):102–109, 2005.

[99] P. J. Tighe, S. J. Badiyan, I. Luria, A. P. Boezaart, and S. Parekattil. Technical communication: robot-assisted regional anesthesia: a simulated demonstration. *Anesthesia and Analgesia*, 111(3):813–816, Sep 2010.

[100] A. L. Trejos, R. V. Patel, and M. D. Naish. Force sensing and its application in minimally invasive surgery and therapy: A survey. *Proceedings of the Institution of Mechanical Engineers, Part C: Journal of Mechanical Engineering Science*, 224(7):1435–1454, July 01 2010.

[101] A. Uneri, M. A. Balicki, J. Handa, P. Gehlbach, R. H. Taylor, and I. Iordachita. New steady-hand eye robot with micro-force sensing for vitreoretinal surgery. In *3rd IEEE RAS and EMBS International Conference on Biomedical Robotics and Biomechatronics (BioRob), 2010*, pages 814–819, 2010.

[102] V. van Hemert tot Dingshof, M. Lazeroms, A. van der Ham, W. Jongkind, and G. Honderd. Force reflection for a laparoscopic forceps. In *Proceedings of the 18th Annual International Conference of the IEEE Engineering in Medicine and Biology Society*, volume 1, pages 210–211 vol.1, 1996.

[103] Lawton N. Verner and Allison M. Okamura. Effects of translational and gripping force feedback are decoupled in a 4-degree-of-freedom telemanipulator. In *Second Joint EuroHaptics Conference, 2007 and Symposium on Haptic Interfaces for Virtual Environment and Teleoperator Systems. World Haptics 2007*, pages 286–291, 2007.

[104] K. Vlachos and E. Papadopoulos. Transparency maximization methodology for haptic devices. *Ieee-Asme Transactions on Mechatronics*, 11(3):249–255, JUN 2006.

[105] C. R. Wagner and R. D. Howe. Force feedback benefit depends on experience in multiple degree of freedom robotic surgery task. *IEEE Transactions on Robotics*, 23(6):1235–1240, 2007.

[106] Christopher R. Wagner, Nicholas Stylopoulos, Patrick G. Jackson, and Robert D. Howe. The benefit of force feedback in surgery: Examination of blunt dissection. *Presence: Teleoperators and Virtual Environments*, 16(3):252–262, 06/01; 2011/11 2007.

[107] Toshikatsu Washio and Kiyoyuki Chinzei. Needle force sensor, robust, sensitive detection of the instant of needle puncture. In *7th International Conference on Medical Image Computing And Computer-assisted Intervention MICCAI 2004*, pages 113–120, 2004.

[108] Z. Wei, G. Wan, L. Gardi, G. Mills, D. Downey, and A. Fenster. Robot-assisted 3d-trus guided prostate brachytherapy: system integration and validation. *Medical physics*, 31(3):539–548, Mar 2004.

[109] M. Yang and JD Zahn. Microneedle insertion force reduction using vibratory actuation. *Biomedical Microdevices*, 6(3):177–182, SEP 2004.

[110] P-L Yen and B. L. Davies. Active constraint control for image-guided robotic surgery. *Proceedings of the Institution of Mechanical Engineers, Part H: Journal of Engineering in Medicine*, 224(5):623–631, May 01 2010.

[111] G. Zeng and A. Hemami. An overview of robot force control. *Robotica*, 15(05):473, 1997.

[112] M. Zhou, D. B. Jones, S. D. Schwaitzberg, and C. G. L. Cao. Role of haptic feedback and cognitive load in surgical skill acquisition. In *51st Annual Meeting of the Human Factors and Ergonomics Society, HFES 2007*, volume 2, pages 631–635. Affiliation: Mechanical Engineering Department, Tufts University, Medford, MA; Affiliation: Department of Surgery, Beth Israel Deaconess Medical Center, Boston, MA; Affiliation: Department of Surgery, Cambridge Health

Alliance, Cambridge, MA; Correspondence Address: Zhou, M.; Mechanical Engineering Department, Tufts University, Medford, MA, 1 October 2007 through 5 October 2007 2007.

[113] M. Zhou, J. Perreault, S. D. Schwaitzberg, and C. G. L. Cao. Effects of experience on force perception threshold in minimally invasive surgery. *Surgical Endoscopy and Other Interventional Techniques*, 22(2):510–515, 2008.

[114] A. Zivanovic and B. L. Davies. A robotic system for blood sampling. *Information Technology in Biomedicine, IEEE Transactions on*, 4(1):8–14, 2000.